

Directed Energy for Planetary Defense

Philip Lubin^{a*} and Gary B. Hughes^b

^aPhysics Department, University of California, Santa Barbara, CA, USA

^bStatistics Department, California Polytechnic State University, San Luis Obispo, CA, USA

Abstract

Directed energy in the form of photons plays an increasingly important role in everyday life, in areas ranging from communications to industrial machining. Recent advances in laser photonics now allow very large-scale modular and scalable systems that are suitable for planetary defense. The fundamental requirements of directed energy planetary defense systems are described here, along with the current state of technological readiness. A detailed design is presented for an orbital planetary defense scheme, called **DE-STAR** for **D**irected **E**nergy **S**ystem for **T**argeting of **A**steroids and **exploR**ation. DE-STAR is a modular phased array of kilowatt class laser amplifiers fed by a common seed and powered by photovoltaics. The main objective of DE-STAR is to use focused directed energy to raise the surface spot temperature of an asteroid to $\sim 3,000$ K, sufficient to vaporize all known substances. Ejection of evaporated material creates a large reaction force that alters the asteroid's orbit. Both standoff (DE-STAR) and stand-on (DE-STARLITE) systems are discussed. The baseline standoff system is a DE-STAR 3 or 4 (1–10 km array) depending on the degree of protection desired. A DE-STAR 4 allows initial engagement beyond 1 AU with a spot temperature sufficient to completely evaporate up to 500 m diameter asteroids in 1 year. Small objects can be diverted with a DE-STAR 2 (100 m), while space debris is vaporized with a DE-STAR 1 (10 m). Modular design allows for incremental development, minimizing risk, and allowing for technological co-development. Larger arrays would be developed in stages, leading to an orbiting structure. The smaller stand-on systems (DE-STARLITE) are appropriate for targets with very long lead times to impact so that a dedicated mission can be implemented.

Keywords

Asteroid impact; Directed energy; Laser phased array; Planetary defense

Introduction

Recent advances in photonics make a scientific discussion of directed energy planetary defense feasible, whereas even 10 years ago it was close to science fiction. High-power lasers are capable of delivering sufficient energy density on a target to melt and vaporize any known material. Laser machining and welding are commonplace in industry, where even refractory metals are directly machined or joined with lasers. Scaling of laser technology has spurred the development of directed energy systems that are capable of delivering high energy density on distant targets. Recent developments have resulted in conversion efficiencies of electrical to photon energy of close to

*Email: lubin@deepspace.ucsb.edu

50 % with powers in excess of 1 kW per (handheld) unit. Additionally, and critical for any phased-array program, such devices can be phase locked. Laser design is rapidly changing and even more efficient devices with higher power density will be available in the near future. High power density allows the contemplation of directed energy systems for large-scale deployment. Inside the Earth's atmosphere, directed energy systems are hindered by atmospheric fluctuations of the coherent beam. A directed energy system deployed above the atmosphere could project a beam through space unfettered by atmospheric interference and thus allows the design of systems that are essentially diffraction limited as the interplanetary medium (IPM) is extremely tenuous and does not affect the laser beam significantly. This chapter describes a feasible design for a future orbiting standoff directed energy system, which is called **DE-STAR** for **D**irected **E**nergy **S**ystem for **T**argeting of **A**steroids and **e**xpl**O**ration (Lubin et al. 2013, 2014; Hughes et al. 2013). The system consists of an array of phase-locked modest power laser amplifiers. By controlling the relative phases of individual laser elements, the combined beam can be directed to a distant target. Lasers are powered by solar photovoltaics of essentially the same area as the laser array. By increasing the array size, it is possible to both reduce the spot size due to diffraction and increase the power. This dual effect allows the system to vaporize elements on the surface of asteroids at distances that are significant compared to the solar system. By raising the flux (W/m^2) on the target asteroid to a sufficiently high level, direct evaporation of the asteroid occurs within the beam. This has two basic effects. First, direct evaporation of the asteroid begins, and given sufficient time, a threatening asteroid could be totally vaporized before hitting the Earth. Second, evaporation at the spot causes a back reaction on the asteroid from the vaporization plume which acts as a rocket, and thus the asteroid can be deflected to miss the Earth. This chapter explores the potential capabilities of the system for mitigating the threat of asteroid impact. Since DE-STAR is a phased array consisting of a very large number of elements, it can simultaneously be used for multiple purposes and is intrinsically a multitasking system. Figure 1 depicts an orbiting DE-STAR system simultaneously engaged in both evaporating and deflecting a large asteroid as well as powering and propelling a spacecraft. As this is a modular system, each DE-STAR is classified by the log of its linear size; thus, a DE-STAR 1 is 10 m, DE-STAR 2 is 100 m, etc. A DE-STAR 4 system will produce a reaction thrust comparable to the Shuttle Solid Rocket Booster (SRB) on the asteroid due to mass ejection and thus allow for orbital diversion of even larger asteroids, beyond several km in diameter, thus allowing for protection from every known asteroid threat. Smaller systems are also extremely useful. For example, a DE-STAR 2 (100 m size array) would be capable of diverting volatile-laden objects 100 m in diameter by initiating engagement at $\sim 0.01\text{--}0.5$ AU (AU = astronomical unit = mean distance from Earth to Sun $\sim 1.5 \times 10^{11}$ m). Smaller objects could be diverted on shorter notice. The phased-array configuration is capable of creating multiple beams, so a single DE-STAR of sufficient size could engage several threats simultaneously, such as a Shoemaker-Levy 9 scenario on Earth. An orbiting DE-STAR would also be capable a wide variety of other functions. Narrow bandwidth and precision beam control would aid narrow search and ephemeris refinement of objects identified with wide-field surveys. Propulsion of kinetic or nuclear tipped asteroid interceptors or other interplanetary spacecraft is possible using the "photon rail gun" mode from direct photon pressure on a spacecraft, propelling a 100 kg craft to 1 AU in 3 days and a 10,000 kg craft to 1 AU in 30 days. A DE-STAR could also provide power to ion propulsion systems, providing both a means of acceleration on the outbound leg and deceleration for orbit. Ideally two systems would provide the ability to "ping pong" spacecraft if this were needed, though this is vastly more challenging. Vaporization and deorbiting of debris in the Earth's orbit could be accomplished with a DE-STAR 1 or 2 system. DE-STAR 3 and 4 arrays may allow standoff interrogation of asteroid composition by observing absorption lines in the blackbody spectrum of a vaporizing surface spot. There are a number of other

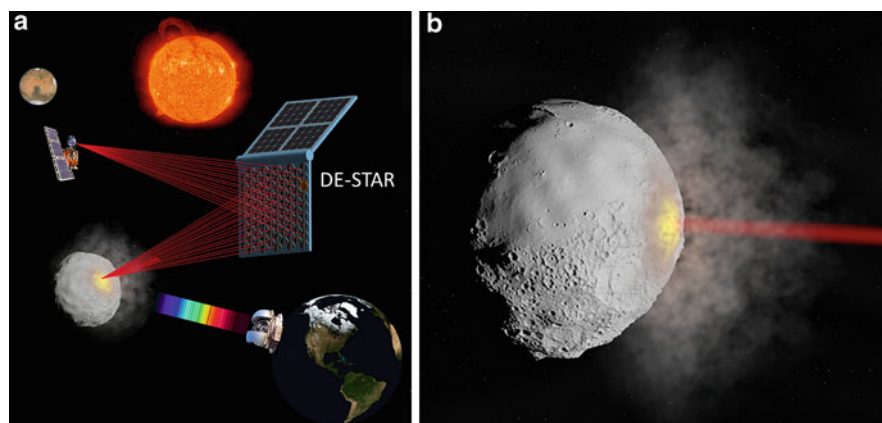


Fig. 1 (a) Concept diagram of an orbiting DE-STAR engaged in multiple tasks including asteroid diversion, composition analysis, and long-range spacecraft power and propulsion. The system consists of an array of phase-locked lasers. By controlling the relative phases of individual laser elements, the combined beam can be directed to a distant target. Lasers are powered by a solar panel of effectively the same area as the laser array. A DE-STAR of sufficient size would be capable of vaporizing elements on the surface of asteroids. Given sufficient time, a threatening asteroid could be vaporized, deflected, or disintegrated prior to impacting Earth. The ability to direct energy onto a distant target renders DE-STAR capable of many functions. Asteroid interrogation may be possible by viewing absorption lines as the heated spot is viewed through the ejected vapor plume. Photon pressure can be used to accelerate (and decelerate) interplanetary spacecraft, among many other possibilities. (b) Visualization with relevant physical phenomenon included at a flux of about 10 MW/m^2 . For comparison, laboratory test setup is shown below in Fig. 24 where the bright high-temperature spot is also visible with about the same flux. The plume density is exaggerated to show ejecta. Asteroid diameter is about that of Apophis (325 m) relative to the laser beam diameter (30 m). Target is at 1 AU

applications as well, including downlink power via mm, microwave, or laser – the so-called Space Power System or SPS mode. The system is a **standoff planetary defense system** that is always ready when needed, and no dedicated mission is needed for each threat, as is the case with other proposed mitigation methods.

The multipurpose aspect of the system allows it to be useful with very high “duty cycle.” The DE-STAR system is inherently modular and scalable, thus allowing a means to build and test smaller units in the lab, on the ground, and in suborbital test flights on balloons. **Each module is modest in size and power and identical allowing for mass production. This is key to cost reduction.** Each element uses only modest laser power, and thus the areal power density is low ($<1 \text{ kW/m}^2$). It is inherently redundant since each module is largely self-contained, and thus failure of modest numbers of elements has little effect. The flux on target (W/m^2) at a fixed distance scales as the d^4 where d is the linear dimension of the array, and thus it increases very rapidly with increased size. This system is useful for many other purposes, which are briefly mentioned in this paper (and discussed in greater detail in other DE-STAR papers).

Other Concepts for Orbit Deflection

The NASA Authorization Act of 2008, Title VIII – Near Earth Objects, Section 804 established a policy with respect to threats posed by Near Earth Objects. The policy includes procedures for notifying federal agencies and emergency response institutions of impending threats. To protect the United States from any object that is expected to collide with Earth, the policy requires the implementation of a deflection campaign, in consultation with international bodies, should one be necessary.

A wide array of concepts for asteroid deflection have been proposed. Several detailed surveys of threat mitigation strategies are available in the literature, including Belton et al. (2004), Gritzner and

Kahle (2004), Colombo et al. (2009), Cuartielles et al. (2007), and Morrison et al. (2002). Currently proposed diversion strategies can be broadly generalized into six categories:

1. Kinetic impactors, with or without explosive charges. An expendable spacecraft would be sent to intercept the threatening object. Direct impact would modify the object's orbit through momentum transfer. Enhanced momentum transfer can be accomplished using an explosive charge, such as a nuclear weapon (e.g., Koenig and Chyba 2007; Melosh and Ryan 1997; McInnes 2004).
2. Gradual orbit deflection by surface albedo alteration. The albedo of an object could be changed using paint (Hyland et al. 2010), mirrors (Vasile and Maddock 2010), sails (Wie 2007), etc. As the albedo is altered, a change in the object's Yarkovsky thermal drag would gradually shift the object's orbit.
3. Direct motive force, such as by mounting a thruster directly to the object. Thrusters could include chemical propellants, solar- or nuclear-powered electric drives, or ion engines (Walker et al. 2005).
4. Indirect orbit alteration, such as gravity tractors. A spacecraft with sufficient mass would be positioned near the object and maintain a fixed station with respect to the object using onboard propulsion. Gravitational attraction would tug the object toward the spacecraft and gradually modify the object's orbit, such as Schweickart et al. (2006) and Lu and Love (2005).
5. Expulsion of surface material such as by robotic mining. A robot on the surface of an asteroid would repeatedly eject material from the asteroid. The reaction force when material is ejected affects the object's trajectory (Olds et al. 2007).
6. Vaporization of surface material. Like robotic mining, vaporization on the surface of an object continually ejects the vaporized material, creating a reactionary force that pushes the object into a new path. Vaporization can be accomplished by solar concentrators (Gibbings et al. 2011) or lasers (Maddock et al. 2007) deployed on spacecraft stationed near the asteroid. One study (Kahle et al. 2006) envisioned a single large reflector mounted on a spacecraft traveling alongside an asteroid. The idea was expanded to a formation of spacecraft orbiting in the vicinity of the asteroid, each equipped with a smaller concentrator assembly capable of focusing solar power onto an asteroid at distances near ~1 km.

Laser Phased Arrays

System Architecture

Planar arrays of phase-locked lasers have been developed in the laboratory. Vorontsov et al. (2009) describe a phased array of densely packed fiber laser collimators. The system utilizes adaptive dynamic phase distortion compensation to accomplish phase locking across the laser array. Other schemes for combining coherent beams have also been described (Fan 2005). The efficiency of laser fiber amplifiers has undergone a remarkable revolution in the last decade resulting from both the telecom industry and the commercial need for high-power solid-state lasers for machining among other tasks. With efficiencies already close to 50 % for the lasers and with solar cells near 50 % efficient, considering such a system is now realistic. **The basic approach is to use existing technology without requiring any “miracles” but with reasonable expectations for modest improvements with an eye toward new devices that may be superior, but the basic fact remains – it is now possible with high efficiency to convert light from the Sun into a highly focused coherent beam capable of planetary scale defense.** It is now inevitable that this will be done and rapid progress with modest costs can begin this process that will lead to a full defensive

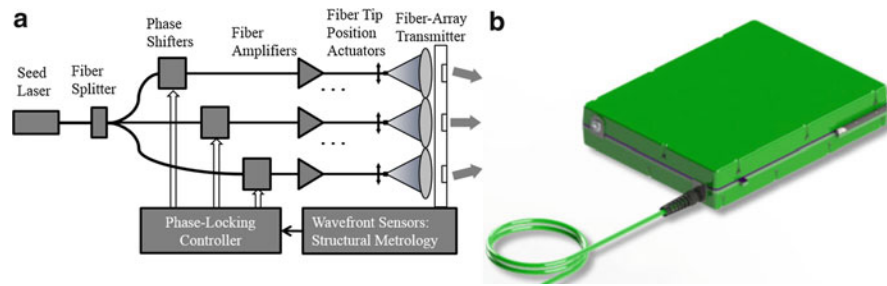


Fig. 2 (a) A system block diagram of the fiber amplifier configuration, based on the work by Vorontsov et al. (2009). Individual beams combine near the target. Here, coarse beam orientation is accomplished by moving individual fiber amplifier tips in relation to the transmitting element. Fine beam steering and beam combination at the target is accomplished by phase control. (b) Existing 1.5 kW Yb-doped fiber amplifier of the baseline design. Size is about $30 \times 40 \times 10$ cm. Only one amplifier is required per 2 m^2 of the system

capability. With efficiencies approaching unity, only modest projected improvements (factor of 2) in efficiency are required to attain a rapid improvement in power density (kW/kg). While current power density is about 0.2 kW/kg using ytterbium (Yb)-doped fiber amplifiers, a relatively rapid roadmap to 1 kW/kg is already in place. In the next decade, an order of magnitude increase in power density is expected. The current DARPA Excalibur program is one example of pursuing high-efficiency fiber-fed lasers. Excalibur goals are multi-kW fiber 1.06 μm wavelength laser amplifiers with a target of >0.2 kW/kg with near 40 % efficiency for the laser amplifier. Efficiency goals are comparable to current LEDs that are already about 50 % efficient. Coincidentally, on the space PV side, the power density is nearly identical at 0.1 kW/kg (ATK UltraFlex) with modest term possibilities for increasing this to 1 kW/kg. Recent work on Inverted Metamorphic Multijunction (IMM) cells promises >0.5 kW/kg. Schematic block diagram for a phased-array laser system based on individual kW-class fiber amplifiers is shown in Fig. 2.

Long coherence length is critical and the existing fiber-based laser amplifiers are already good enough (depending on the mode in which they are operated), though new advances are becoming available to allow the SBS (stimulated Brillouin scattering) limit to be extended with even longer coherence lengths. With the current technology a DE-STAR 2 program could be started leading to launch and possibly a DE-STAR 3. A conservative and logical approach is possible, rapidly building smaller and much lower cost units (DE-STAR 0 and 1), testing on the ground, and then, as technology catches up and technological and system problems arise and are solved move to larger systems, eventually leading to orbital testing and scaling up to the full defensive goal. The system is not binary in that small systems have immediate applications (e.g., DE-STAR 1 space debris) as larger systems are being developed for comet and small asteroid protection (DE-STAR 2) leading eventually to a DE-STAR 3 or 4.

As a goal, studies have been performed to assess the feasibility of a system possessing the capability to evaporate, prior to impact, asteroids in the size range 150 m to 1 km, and with typical orbital closing speeds. These stated capabilities drive system requirements into the multi-km-class array size for both the diffraction limit of the optics and the power required. As a specific example, one objective might be seeking to evaporate an Apophis-class asteroid (325 m diameter) with a **worst-case** assumption of complete chemical binding and less than 1 year to evaporate the entire boloid, with a desired interdiction starting at 1 AU. A 10 km DE-STAR system would be capable of meeting the stated goal as shown in the calculations presented below. It is also fortuitous that the same size system required to form a small spot on the distant asteroid from the diffraction limit, assuming a wavelength near 1 μm , is also about the same size as needed to power the laser amplifiers

in order to raise the flux to the evaporation point from converting sunlight that falls on the DE-STAR into electricity. At the Earth's orbit, the "solar constant" is about $1,400 \text{ W/m}^2$ or 1.4 (140) GW of sunlight on a 1 (10) km-sized solar array. This is sufficient to power the entire system and no additional power is needed. This also forms a very large potential for an SPS system to send excess power to the Earth. By utilizing a filled array of solar-powered phase-locked lasers, there is a near-ideal convergence of size required both to power the system and to produce the diffraction-limited beam needed to begin vaporization. Baseline calculations are developed using a $1.06 \mu\text{m}$ wavelength, to produce sufficient flux at 1 AU that will sustain evaporation, which requires greater than approximately 5 MW/m^2 flux at target. As stated existing Yb laser fiber amplifiers at $1.06 \mu\text{m}$ wavelength have efficiencies near 40 %. Space solar PV has efficiency of about 35 % in one Sun (not concentrated) with near 50 % when concentrated. Modest efficiency improvements are assumed for both laser and PV to 70 % which is not unreasonable in the realistic time scale of a full DE-STAR 4 system. Overall conversion efficiency of sunlight to laser power of about 50 % is assumed, resulting in approximately 0.7 GW/km^2 of laser power. For a 1 km system, laser power would be 0.7 GW, while a 10 km system would have laser power of 70 GW, which is more than sufficient for meeting the stated goal of surface vaporization at 1 AU of all known materials. One major advantage of a phased array is that multiple independent beams can be produced, so multiple targets or efforts can be simultaneously engaged. For reference, 70 GW is the equivalent of about 1.4 MT (megatons TNT – $1 \text{ MT} \sim 4.2 \times 10^{15} \text{ J}$) per day or about 500 MT per year of potentially deliverable energy, a significant portion of the total currently active US nuclear arsenal. Note that in the process there is also 100 GW of electrical energy produced or the equivalent of about 100 large utility nuclear reactors. This would allow a very large SPS if needed.

For DE-STAR, launch mass is critical in the costing analysis, so while the required efficiency is already effectively available, the power mass density must increase significantly. Solar PV cells can be extremely thin and low areal mass through focusing with thin film mirrors on solar PV may allow the lowest densities. For example, if $10 \mu\text{m}$ thick PV could be produced (this is more of a mechanical issue as thinner films already exist on plastic), a 10^4 m PV array would have a mass of about $3 \times 10^6 \text{ kg}$. The current issue for many space solar cells is the charged particle degradation which is currently met with a "cover glass" on each side of about $100 \mu\text{m}$. If laser power density of 10 kW/kg could be reached ($50\times$ higher than current), then 70 GW of fiber lasers would be $7 \times 10^6 \text{ kg}$. This mass does not represent the entire DE-STAR system, but the scale is not outrageous. **10 kW/kg for laser mass density over 20 years is a goal, but even the existing 0.2 kW/kg density allows up to nearly a DE-STAR 3** using existing launcher capability. For reference, the International Space Station (ISS) mass is about $0.5 \times 10^6 \text{ kg}$ with much more than this being lifted into orbit as much of it was also returned in Shuttle missions. Conservatively, it is already possible to launch few $\times 10^6 \text{ kg}$ class space mission, an example being the ISS. Either heavy lift chemical launchers would be needed to loft DE-STAR 4 modules or a bootstrap ground-based DE-STAR-driven hybrid booster would be required. The modules are being designed around the existing heavy lift fairing size allowing for a 3–4 m diameter class module. The modules can be quite thin and stacked during launch and assembled in orbit. Since the system is a phased array, the structure does not need the structural integrity of a conventional mirror but rather must be stiff enough to have vibration modes that are below the metrology servo loop bandwidth as phase control is not handled by keeping the structure stiff but rather by measuring the relative position of each element adjusting the phase shifter in each amplifier to keep the beam on the target.

While the baseline design is run in a continuous fashion (CW mode), it is also possible to run the system pulsed if needed, though short pulses are more problematic to phase properly. Extensive simulations and some laboratory testing indicate the debris field caused by the mass ejection should

not significantly interfere with the incoming laser as the ejecta density is quite low (maximum near the surface is estimated to be 10^{-2} kg/m³ and rapidly falling off due to the near isotropic ejecta emission into the space vacuum). Typical molecular ejecta speeds are 1–2 km/s. A reality check is to watch laboratory tests in one atmosphere at up to 40 MW/m² or to view a video of a laser milling machine. The system is much like a laser-heated target in a semiconductor fabrication system.

Thermal Dissipation: The average thermal load (to dissipate) of the system (independent of size) is about 500 W/m² which is approximately that of a person (or the Earth). It is equivalent to a 300 K blackbody. The average thermal load is extremely low. The average laser power is also quite low, being about 700 W/m² which is less than the solar “constant” on the surface of the Earth which is about 1,000 W/m². You could literally walk in front of the system when operational and not be harmed (laser glasses are recommended however).

Optical Design: The optical design of a phased array is different than that of a classic optical telescope in that the phasing to achieve constructive interference (which is what allows the image to form) is not done with mechanical alignment as it is in a mirror or lens (where every part of the mirror is essentially a part of the overall “phased array”), but rather the phasing is done by adjusting the phase at each sub-element to achieve constructive interference at the target. The design is an extremely narrow field of view system, and thus many of the constraints of a classical optical system do not apply. The array can be any shape, for example. The system is also extremely narrow bandwidth so thin film holographic grating diffractive “lenses” become viable. For simplicity the design will be roughly planar with each sub-element being either a small reflector or possibly a thin film holographic lens. The latter has been tried in some narrowband receiving mode systems, and extremely low areal densities have been achieved. This is an area where further work is needed to decide on the optimum approach. The design is a large number of identical low-power (700 W/m²) modules that lend themselves to mass production. Ultralow-mass holographic thin film large area “lenses” are particularly attractive, but SiC- or CFRP-replicated reflective optics may be suitable with refinement to lower the mass. In the current baseline, each element has a single fiber amplifier that feeds an optical element. A single 1 kW amplifier can feed a 1.5 m² optic (mirror or lens). Coarse pointing could be accomplished using fiber tip position actuators behind the lens or mirror as appropriate. A fallback option would be to gimbal each element, though this is more complex. Fine pointing is done with electronic phase adjusters at each amplifier input. The phase is also compared at the output and between elements. The metrology of the entire structure becomes a key part of the servo system. There have been a number of orbital programs looking at extremely high-precision laser metrology over long baselines. The most extreme is the LISA gravitational wave detector that sets a metric of 20 pm resolution over 5×10^9 m baseline. This is vastly better than required for DE-STAR. Metrology of about 0.1 μ m ($\lambda/10$) is required over 10 km for the full DE-STAR 4. Similarly the AMD-MOST program has achieved 1 nm resolution over roughly 10 m baselines (limited by the vacuum chamber for testing). At longer wavelengths the Event Horizon Telescope has phased locked 1.3 mm wavelength telescopes across the globe (10^7 m baseline) and achieved 0.1 nrad beam formation or the same as the current goal. The RadioAstron, a Russian and Earth long baseline interferometer, has produced fringes corresponding to 0.04 nrad. Note that since the optical $F\#$ is very large ($\sim 1.5 \times 10^7$ for a DE-STAR – 1 AU target), the asteroid is far away and hence the beam is nearly parallel at the target with a large “depth of focus” $\sim F\#^2 \lambda \sim 2 \times 10^8$ m. The $F\#$ (F number) is the ratio of L/d , where L is the target distance and d is the DE-STAR size.

There are a number of challenges to the optical design and the targeting servo system that need to be explored. Asteroids are dynamic, and while motion in angle may be small relative to a viewing angle from Earth, it can still be significant. Typical asteroid moves at 10–30 km/s, and with a 30 m beam, this is 300–1,000 beam diameters per second in the worst case. The system will be moving in

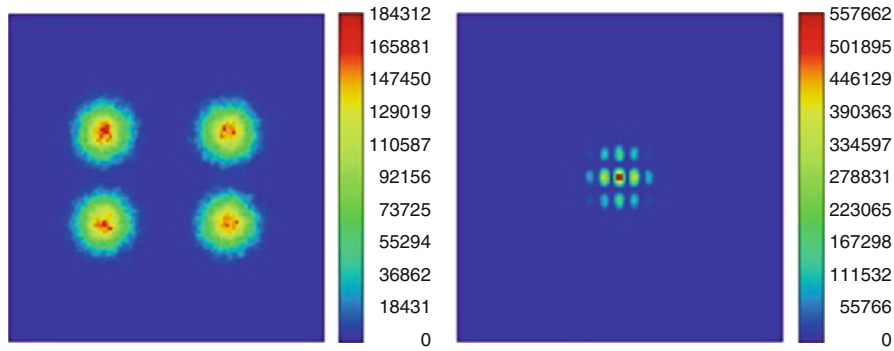


Fig. 3 Coherent beam combining of a 2×2 laser array in Zemax. The four individual elements are shown on the *left*, and then when combined, the central peak is intensified and the sidelobes are suppressed. With additional elements, the peak will grow and the sidelobes will decrease. The baseline uses a filled close-packed array to minimize sidelobes and to maximize the central peak

its orbit, the Earth is moving, etc. There are a lot of issues to be worked out. The Hubble Space Telescope has about a 35 nrad pointing stability over 24 h as an example. Better than 0.1 nrad pointing is ideally required (the current experimental beam is 0.2 nrad full-width, half max (FWHM) for a DE-STAR 4), though, as shown below in the simulations, there is some latitude in this. Optical designs have been started; Fig. 3 shows a simple 2×2 array as an example using coherent beam combining in Zemax. A far-field beam pattern simulation, based on beam propagation equations, is shown in Fig. 4.

Laser Versus Mirror

In general, the DE-STAR system can be described as “laser machining” on a solar system scale. While laser machining is common in everyday life, from processing of clothes to cars, it is not common to think about systems that can machine on solar system scales. One of the first questions asked is, “why not use a mirror to form an intense spot rather than convert from sunlight to electricity to laser light?” The answer is simple. If the Sun were a point source, it would be possible to do precise beam formation and targeting, but the Sun is not a point source and the conservation of phase space (Liouville’s theorem) prevents beam formation without the use of a mirror about the size of the distance to the target. For an object at 1 AU, targeting with a mirror would require a reflector about the size of the solar system! Stated more precisely, the flux for a spot on the target F_{sp} when using a mirror of a given $F_{\#} = \text{focal length/diameter}$ focusing a source whose surface flux is F_s will give

$$F_{sp} = \frac{\epsilon F_s}{4F_{\#}^2}$$

$$F_{sp} = \sigma T_{sp}^4 = \frac{\epsilon}{4} T_s^4 F_{\#}^{-2} \rightarrow T_{sp} = \left(\frac{\epsilon}{4}\right)^{1/4} F_{\#}^{-1/2} T_s$$

where T_{sp} is the spot temperature assuming only radiation equilibrium (no mass ejection), T_s is the source surface temperature, and ϵ is the efficiency of coupling the photons to the target. An assumption of $\epsilon = 1$ is used for simplicity. The Sun is roughly equivalent to a 5,700 K blackbody with a surface flux of about 60 MW/m^2 . To achieve good efficiency for rocky materials typical of asteroids, flux at the target needs to be greater than about 10 MW/m^2 which requires a mirror with an $F_{\#} \sim 1$ or the diameter about the same as the target distance as mentioned above. This is also one reason why bringing mirrors to an asteroid requires that mirrors also have an $F_{\#} \sim 1$ so that the mirror

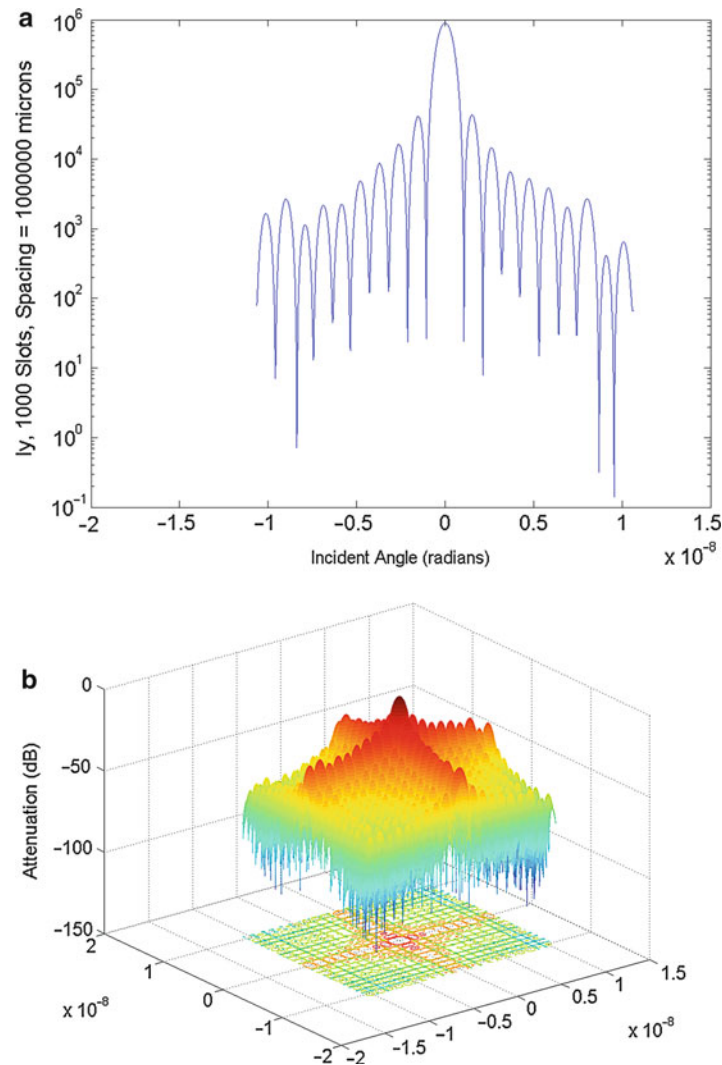


Fig. 4 Simulation of $1,000 \times 1,000$ array of 1 m sub-apertures. (a) 1D cut and (b) the full 2D pattern. Simulation includes the effects of uncorrelated phase noise equal to a WFE of $\lambda/10$ per element. For WFE phase noise less than about $\lambda/6$, there is little effect on the final beam pattern with the primary effect being main beam power being spread into the sidelobes (Hughes et al. 2014)

must be very close to the asteroid which can be very problematic for a variety of technical reasons. Comets require much lower temperature and flux to evaporate, but since the target flux drops inversely with $F_{\#}^2$ and the spot temperature drops inversely as $F_{\#}^{1/2}$, even an ice asteroid would require an $F_{\#} < \sim 300$, so standoff planetary defense against comets with mirrors is not feasible; mirrors brought to comets and asteroids with large percentages of volatile compounds are feasible if it is possible to bring the mirror to the target

Laser Arrays: It is possible to analyze the case of a simple square array as an extension of a series of rectangular apertures. The circular case is very similar. More complex systems with realistic phase noise and pointing errors are analyzed in Lubin et al. (2014). For the simple case of a square array of

side d and target distance L assuming **only cooling by radiation transfer** (the case of mass ejection is considered below), the following definitions and relations hold:

d = laser array size (m)
 P_E = electrical power (W)
 ϵ_L = laser efficiency (wall plug)
 P_L = laser power (W)

$$P_L = \epsilon_L P_E \text{ (W)}$$

λ = laser wavelength (m)
 L = target distance (m)
 D = spot size (m)

$D = 2L\lambda/d = 2F_{\#}\lambda$ = spot diameter
 where $F_{\#} = \frac{L}{d}$

ϵ_B = beam power fraction in spot = beam efficiency
 F = flux at target (W/m^2)

$$F = \frac{\epsilon_B P_L}{D^2}$$

ϵ_T = Target Absorption coefficient = $1 - \alpha$ at wavelength λ of laser
 α = albedo (reflection) which includes surface and melt/vapor reflection

Solving for the target parameters gives the following relations (note the scaling laws):

$$F = \frac{\epsilon_B P_L}{D^2} = \frac{\epsilon_B \epsilon_L P_E}{(2L\lambda/d)^2} = \frac{\epsilon_B \epsilon_L P_E d^2}{4L^2 \lambda^2} = \frac{\epsilon_B P_L d^2}{4L^2 \lambda^2}$$

$$\propto P_L, d^2, L^{-2}, \lambda^{-2}$$

$\epsilon_T F = \sigma T^4$ = target adsorbed flux from laser = radiated flux

Here we assume only radiation balance and no mass ejection

The real case of mass ejection dominance is discussed below

$$T = \left(\frac{\epsilon_T F}{\sigma}\right)^{1/4}$$

$$T = \left[\frac{\epsilon_T \epsilon_B \epsilon_L P_E d^2}{4L^2 \lambda^2 \sigma}\right]^{1/4} = \left[\frac{\epsilon_T \epsilon_B P_L}{4\sigma}\right]^{1/4} \left(\frac{d}{L\lambda}\right)^{1/2}$$

$$\propto P_L^{1/4}, d^{1/2}, L^{-1/2}, \lambda^{-1/2}$$

$$L = \sqrt{\frac{\epsilon_T \epsilon_B \epsilon_L P_E}{4\sigma}} \frac{d}{T^2 \lambda} = \sqrt{\frac{\epsilon_T \epsilon_B P_L}{4\sigma}} \frac{d}{T^2 \lambda}$$

$$\propto P_L^{1/2}, d, T^{-2}, \lambda^{-1}$$

$$P_L = \frac{4L^2 \lambda^2 \alpha T^4}{\epsilon_T \epsilon_B d^2}$$

$$\propto L^2, \lambda^2, T^4, d^{-2}$$

Solving for T and D for the general case of an arbitrary-sized array, power, and target distance gives

$$T(\text{K}) \approx 8,160 (\epsilon_T \epsilon_B)^{1/4} P_L^{1/4} (\text{kW}) d^{1/2} (\text{m}) L^{-1/2} (\text{km}) \lambda^{-1/2} (\mu)$$

where $F_{\#} = \frac{L}{d}$

$$D(\text{mm}) = 2 L(\text{km}) \lambda(\mu) d^{-1} (\text{m})$$

$$D(\mu) = 2 F_{\#} \lambda(\mu)$$

$$L(\text{km}) = 66.4 (\epsilon_T \epsilon_B)^{1/2} P_L^{1/2} (\text{kW}) d(\text{m}) T^{-2} (10^3 \text{K}) \lambda^{-1} (\mu)$$

$$P_L(\text{kW}) = 2.27 \times 10^{-4} \frac{L^2 (\text{km}) \lambda^2 (\mu) T^4 (10^3 \text{K})}{\epsilon_T \epsilon_B d^2 (\text{m})}$$

$$P_L(\text{kW}) = 2.27 \times 10^{-4} \frac{L^2 (\text{km}) \lambda^2 (\mu) T^4 (10^3 \text{K})}{\epsilon_T \epsilon_B d^2 (\text{m})}$$

For $L = 1 \text{AU}$:

$$D(\text{m}) = \frac{3 \times 10^5}{d(\text{m})} \lambda(\mu)$$

DE-STAR with PV Array Equal to Laser Array Size: For simplicity in designing the baseline system, the assumption is that the PV array would be the same size as the laser array. In practice this is not necessary, but it yields about the right amount of power needed to begin interdiction at 1 AU for a class 4 system. In the case of the PV array being the same size as the laser array, the previous equations can be simplified. It is possible to solve for the flux on target and equivalent radiation transfer temperature at the spot – again assuming only radiation equilibrium and no mass ejection:

$$F = \frac{P_L}{D^2} = \frac{K d^2 \epsilon_P \epsilon_L \epsilon_B d^2}{4 L^2 \lambda^2} = \frac{K d^4 \epsilon_P \epsilon_L \epsilon_B}{4 L^2 \lambda^2}$$

ϵ_P = PV conversion efficiency

ϵ_T = target absorption = $1 - \alpha$ where α = albedo

ϵ_B = the beam eff (frac in spot)

ϵ_L = the laser conversion efficiency (“wall plug” efficiency)

K = “solar constant” in space near Earth $\sim 1,361 \text{ W/m}^2$ at solar minimum and about $1,362 \text{ W/m}^2$ at solar maximum.

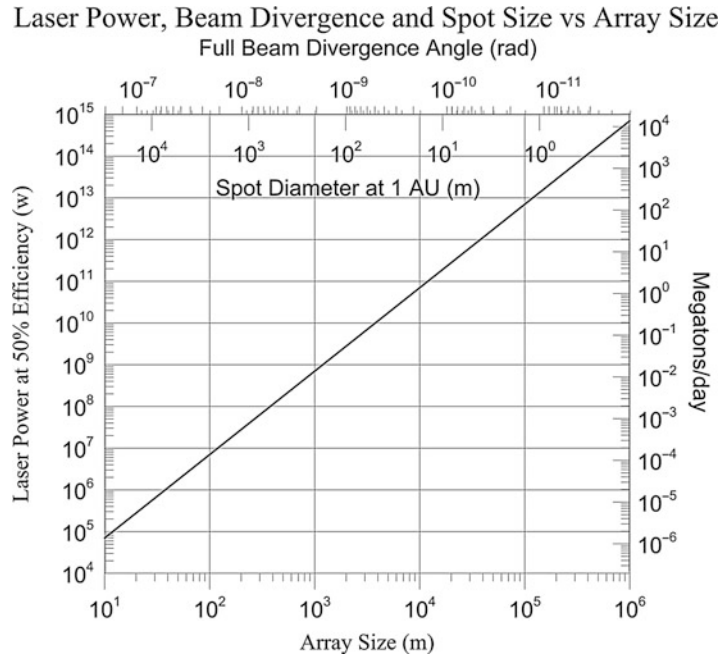


Fig. 5 DE-STAR laser power, diffraction-limited beam divergence, and spot size at target engagement of 1 AU

Radiated flux is set equal to absorbed laser flux:

$$F = \sigma T^4 = \epsilon_T F$$

$$T = \left(\frac{F}{\sigma}\right)^{1/4} = \left[\frac{Kd^4 \epsilon_P \epsilon_L \epsilon_B}{4L^2 \lambda^2 \sigma}\right]^{1/4} = \frac{d}{\sqrt{2L\lambda}} \left[\frac{K \epsilon_P \epsilon_L \epsilon_B}{\sigma}\right]^{1/4}$$

$$d = T \sqrt{2L\lambda} (K \epsilon_P \epsilon_L \epsilon_B / \sigma)^{-1/4}$$

$$L = \frac{d^2}{2T^2 \lambda} (K \epsilon_P \epsilon_L \epsilon_B \epsilon_T \sigma)^{1/2}$$

As an example, a class 4 system has $F\# = \frac{L}{d} \approx 1.5 \times 10^7$ for a target at $L = 1$ AU with $d = 10^4$ m and achieves a spot temperature, if radiation limited, in excess of 6,000 K and delivers more than 1 MT/day equivalent. Figure 5 summarizes the above calculations for various values of array size and target distance.

Coherence Length Requirements: For a phased array to work properly, the light must be coherent over a time and thus length scale sufficient for all elements to be able to interfere. The coherence length required can be calculated by determining the length difference between the various elements with the most extreme case being the conservative limit.

For a planar array of size d and a target of distance L away, the path length difference between the central beam and the outermost beam is $\delta \sim d^2/8L = d/8 F\#$ for the case of a target that is normal to the plane of the phased array. Moving off normal, the path length difference is $\delta = 1/2 d \sin(\theta)$, where θ is the angle of the target off the normal. The worst case is at right angles ($\theta = \pi/2$) where $\delta = d/2$. If there are controllable optical delay lines, then these issues are drastically mitigated, but it is preferable to have long coherence length, so delay lines are needed. For a target at $L = 1$ AU ~ 1.5

$\times 10^{11}$ m and a DE-STAR 4 with $d = 10^4$ m that $F\#$ is $\sim 1.5 \times 10^7$ - $\delta \sim 80 \mu\text{m}$ corresponding to a coherence time $t_c = \delta/c \sim 0.3$ ps. For the worst case of $\delta = d/2$, the equivalent $t_c = \delta/c \sim 17 \mu\text{s}$. The laser coherence time must be greater than these times. The “coherence bandwidth” of the current Yb fiber amplifiers is intrinsically about 5–10 kHz (with corresponding coherence times $t_c \sim 100 \mu\text{s}$ or comfortably longer than the stated worst case. For amplifiers run at their highest power level, this “coherence bandwidth” is generally artificially broadened to about 10 GHz (100 ps) in order to overcome what is known as the stimulated Brillouin scattering (SBS) limit that limits the amplification power. This is well above the normal incidence case but allows extremely little pointing margin. For example, even a 1° pointing difference will give a path length difference of $\delta = 1/2 d \sin(\theta) \sim 90$ m with a corresponding coherence time $t_c = \delta/c \sim 300$ ns. When the amplifier is run at a few hundred watts versus kilowatts, the “coherence bandwidth” is about 5–10 kHz or less as above. The solution to this is to run at normal incidence (not really a good option), add path delay lines (also not a good option in general), or run the amplifiers well outside the SBS limit where the coherence time is longer. The latter is the preferred option. There is technology that has been developed that appears to allow the Yb amplifiers to run at both relatively high power and with long coherence time. This is one of the development items on the roadmap. Since volume (as opposed to mass) is not as much of an issue, there may be a trade space that can be exploited to allow for better performance. Note that the deviation of the planar array from a sphere with radius $R = L$ is $\xi = d^2/8R = d^2/8L \sim 80 \mu\text{m}$ and deviation of the array plane from a classic optic with focal length $f = L$ is $\xi = d^2/16f = d^2/16L \sim 40 \mu\text{m}$. The array is indeed quite planar!

Space Qualification Issues: The DE-STAR system is a complex system of both power conversion (solar to electrical to laser) and metrology, targeting among many others. Solar PV is a mature technology, and the space qualification and “rad hardening” issues are understood. The situation for fiber amplifiers needs to be addressed as a part of the roadmap. Much of this can be done on the ground in accelerator beam lines, and some early long-term space exposure will help with determining what issues, if any, are critical to address in this area. The long-term exposure to radiation is not well understood for fiber amplifiers and needs to be addressed. Rad hardening of thin film holographic lenses also needs to be addressed, as does lowering the areal mass of space PV which is often dominated by the glass used to reduce charged particle (mostly electron) damage.

System Requirements to Evaporate Asteroids

It is possible to calculate the energy required to melt and vaporize the various materials that are common in S-type (Si-rich), C-type (carbon-rich), and M-type (metal-rich) asteroids. Comets are much easier to vaporize in that they do not require a high temperature to begin significant mass ejection. The gravitational binding energy of a molecule to a typical asteroid is very small and is negligible compared to the chemical binding energy. The chemical bonding energy that requires heating of the spot to high temperature can be expressed through the heat of vaporization. The heat of fusion (melting) is a small fraction of the heat of vaporization. Models have been developed to explore the thermal interaction between the laser and asteroid in three ways. The first is a simple analysis based on power only with a flux equivalent to about a 6,000 K blackbody. The second method uses detailed calculations of the vapor pressure versus temperature for every element and many of the estimated compounds that are thought to make up asteroids. This is a quasi 2D analysis in that it includes radiation emission and mass ejection but ignores thermal conduction. The third method uses all the calculations from the second method but uses a full 3D finite element analysis (FEA) of spherical (any shape is possible) asteroids with various thermal conductivities. All three methods give essentially the same answers, which the calculations confirm with increasingly sophisticated simulations. The final method is a laboratory test system that uses a 19-element laser

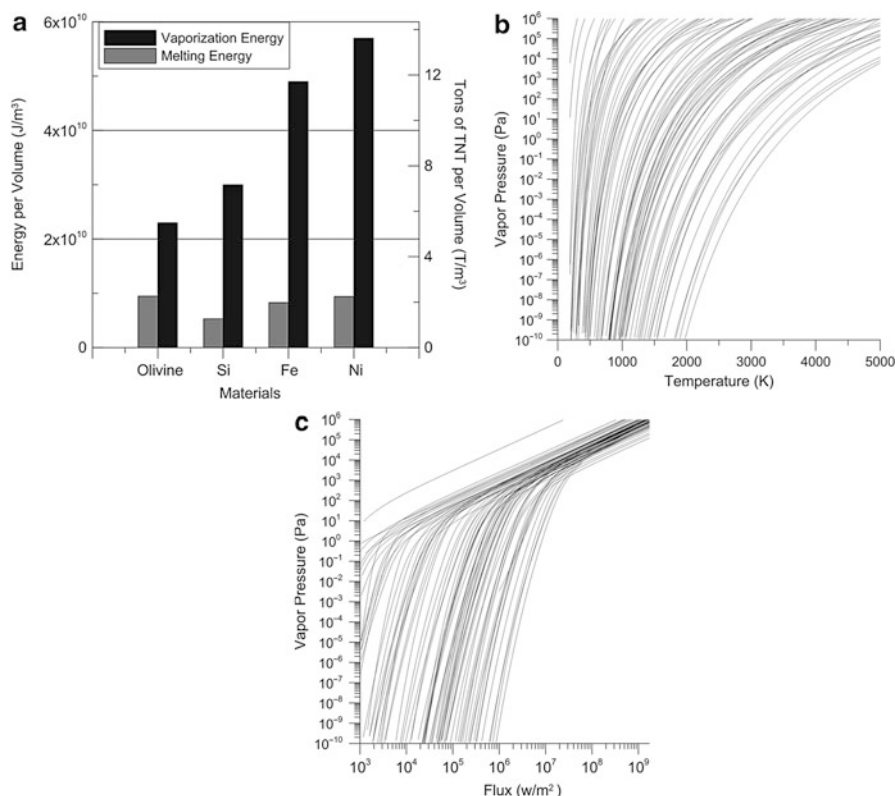


Fig. 6 (a) Melting and vaporization energy per unit volume for S-type (Si-rich) asteroids. (b) Vapor pressure versus T for virtually all elements on the periodic table (93 are modeled). (c) Vapor pressure versus target flux for the same 93 elements. The upper outlier is Mercury

array to produce a spot flux similar to that of the full DE-STAR 4 at 1 AU, namely, about 40 MW/m², and targets “rock” samples with similar compositions to asteroids. This testing has begun and will continue over the next year to cross-check the simulations for evaporation rates, mass ejection densities, and plume thrusts among other parameters. As expected, when the flux exceeds about 2 MW/m², most materials begin to significantly vaporize.

The energy required to melt an asteroid is given by the heat of fusion and required increase in temperature to bring it to the melting point from (assumed) initial low-temperature starting point. In practice this is small compared to the heat of fusion and heat of vaporization. The typical energy per m³ is of order 10¹⁰ J to vaporize most materials. This can be seen in Figs. 6 and 7, which show models of the vapor pressure in pascals (N/m²) versus T and versus target flux for 93 elements. In addition models are shown for four common asteroid molecular compounds. Even vapor pressures of 10³ Pa (0.01 atmospheres) correspond to enormous reaction forces on the asteroid and large mass ejection rates. While an asteroid of solid tungsten is not expected, it would still be possible to mitigate it. Contrary to the small iron-rich meteorites that are found on the ground, a more typical asteroid looks more like the lunar surface and has quite low thermal conductivity and is thought to be a “rubble” pile in many cases, particularly for larger (greater than a few hundred meters) asteroids. The worst case of complete chemical binding (i.e., solid) is assumed. In many cases asteroids will have significant low-temperature volatile materials that may make mitigation much easier. Asteroids are also molecular rather than atomic in species in general, but the conclusion is the same; namely, at temperatures around 2,000–3,000 K or target fluxes of 10⁶–10⁸ W/m², all known materials will undergo vigorous evaporation. What is critical is to increase the spot flux to the point where

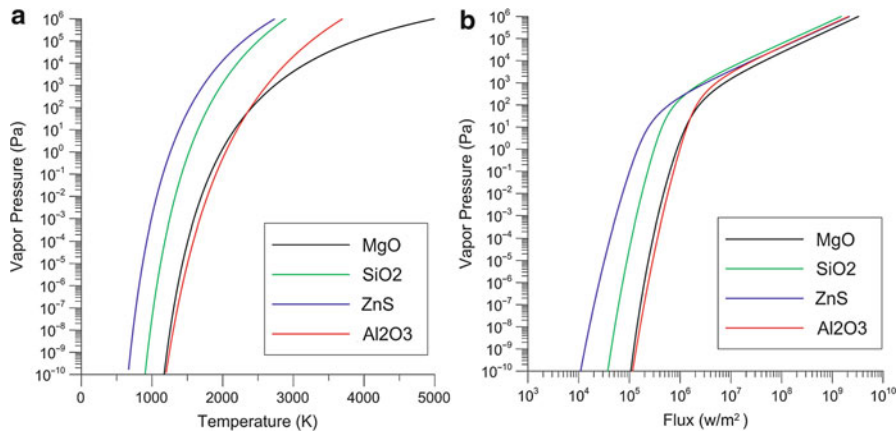


Fig. 7 (a) Vapor pressure versus T for four common high-temperature asteroid compounds. (b) Vapor pressure versus target flux for the same found compounds. Note that at temperatures of 2,000–3,000 K or fluxes of about 10 MW/m^2 , the vapor pressure and hence mass ejection rates are very high

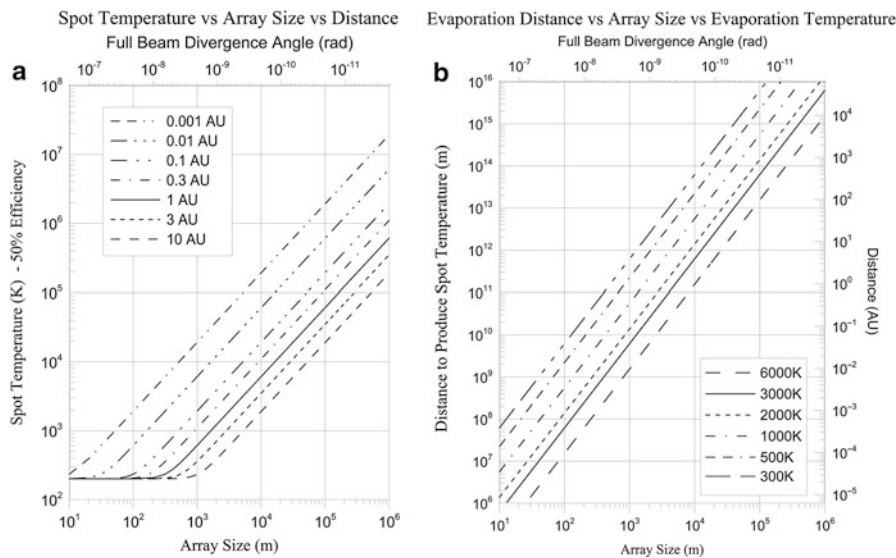


Fig. 8 (a) Spot temperature versus DE-STAR array size for various target distances from 10^{-3} to 10 AU, including average solar illumination on asteroid (sets lower limit on asteroid or comet temperature). (b) Distance to target versus array size for various spot temperatures from 300 to 6,000 K. At 300 K, icy comets become targets, while at 6,000 K (hotter than Sun), no known material survives

evaporation becomes large. It is not sufficient to simply apply a large amount of total power; there has to be a large flux to initiate evaporation.

Once the material properties of the targets are understood (Binzel et al. 2009), it is possible to design a system that is capable of evaporating them and in this process divert them due to the large plume thrust generated. Figure 8 illustrates at what distances it is possible to begin to engage targets of differing compositions. For example, a comet will begin evaporation at much lower flux than a rocky asteroid and thus engage them at much lower total power levels and hence smaller systems or at much larger distances. These simulations assume the Sun is also illuminating the targets which accounts for the lower-temperature limit. This is approximate as it depends on the target reflectivity and orbit. The Sun does not have a significant effect except in the case of comets.

Escape Speed and Temperature

It is possible to calculate the gravitational binding energy and thus the escape speed and equivalent escape temperature as follows. The equivalent temperature for escape is

$$\frac{1}{2}mv^2 = GMm/R = \frac{3}{2}kT$$

$$v_{\text{escape}} = (2GM/R)^{1/2}$$

$T_{\text{esc}} = \frac{2GMm}{3kR}$, where m is the molecular/atomic mass (kg), M is the asteroid mass (kg), R is the asteroid radius.

Assume constant density ρ (kg/m³):

$$M = \frac{4}{3}\pi R^3 \rho$$

$$v_{\text{esc}} = (2GM/R)^{1/2} = \left(2G\frac{4}{3}\pi R^3 \rho/R\right)^{1/2}$$

$$v_{\text{esc}} = R\sqrt{\frac{8\pi}{3}G\rho} \text{ (m/s)}$$

$$v_{\text{esc}} = 2.36 \times 10^{-5} \sqrt{\rho} R$$

$$T_{\text{esc}} = \frac{8\pi}{9k} G\rho m R^2 = 1.35 \times 10^3 \rho m R^2$$

Detailed Thermal Modeling

Thermal modeling is critical. Three approaches are presented here, and all yield consistent results. The basic equations are derived from energy conservation where we now also include the critical mass ejection term.

Power in (laser) = power out (radiation + mass ejection) + $\frac{dU}{dt}$, where U = asteroid internal energy and $\frac{dU}{dt}$ is effectively from conduction. In the steady state $\frac{dU}{dt} = 0$,

$$P_{\text{in}} = P_{\text{out}} + \frac{dU}{dt} \text{ with } U = \int \rho c_v dv, \text{ where } c_v = \text{specific heat (J/kg-K):}$$

$$\begin{aligned} F_L &= \text{Laser Flux-in} && \text{W/m}^2 \\ F_{\text{rad}} &= \text{Radiation Flux-out} && \text{W/m}^2 \\ F_{\text{ejecta}} &= \text{Ejecta Flux -out} && \text{W/m}^2 \\ F_{\text{cond}} &= \text{Thermal Conduction-in} && \text{W/m}^2 \end{aligned}$$

$$\begin{aligned} P_{\text{in}} &= P_{\text{rad}} + P_{\text{Ejecta}} + P_{\text{cond}} \\ \oint (\bar{F}_L - \bar{F}_{\text{rad}} - \bar{F}_{\text{Ejecta}} - \bar{F}_{\text{cond}}) \cdot \hat{n} dA &= 0 \\ &= \int \nabla \cdot (\bar{F}_L - \bar{F}_{\text{rad}} - \bar{F}_{\text{Ejecta}} - \bar{F}_{\text{cond}}) dv = 0 \end{aligned}$$

Locally,

$$\bar{F}_L = \bar{F}_{\text{rad}} + \bar{F}_{\text{Ejecta}} + \bar{F}_{\text{cond}}$$

$$\bar{F}_{\text{rad}} = \sigma T^4 \hat{n}$$

$$\bar{F}_{\text{Ejecta}} = \Gamma e H_v \hat{n} = M^{1/2} (2\pi RT)^{-1/2} \alpha_e 10^{[A-B/(T+C)]} H_v \hat{n}$$

$$\begin{aligned} |\bar{F}_{\text{rad}}| &= \sigma T^4 \\ |\bar{F}_{\text{cond}}| &= K \nabla T \\ |\bar{F}_{\text{Ejecta}}| &= \Gamma e * H_v \end{aligned}$$

where k_T is the thermal conductivity (which can be position and temperature dependent) and Γe is the mass ejection flux ($\text{kg/m}^2\text{-s}$) and H_{eff} is the effective heat of vaporization (J/kg) (here the heat of fusion and integrated specific heat are also included, $H_{\text{eff}} = H_v + H_f + \int_{T_a}^{T_v} C_v dT$). In some cases the material will directly sublime into the vacuum. H_f is typically a small fraction of H_v , so for practical purposes it is a good approximation to use $H_{\text{eff}} \sim H_v$:

$$\Gamma e = \frac{M \alpha_e (P_v - P_h)}{\sqrt{2\pi MRT}} = M^{1/2} (2\pi RT)^{-1/2} \alpha_e (P_v - P_h)$$

where M = molar mass (kg/mol)

P_v = vapor pressure (Pa)

P_h = ambient vapor pressure (Pa) = 0 in vacuum

α_e = coef. of evaporation $0 \leq \alpha \leq 1$

Models are given for the vapor pressure for each element and compound using a semi-analytic form known as Antoine coefficients where the vapor pressure and temperature T are related by:

$\text{Log } P_v = A - B/(T + C)$, where A , B , and C are the Antoine coefficients and are unique to each element and compound. These form the basis for Figs. 6 and 7.

Hence,

$$P_v = 10^{[A-B/(T+C)]}$$

$$|\bar{F}_{\text{Ejecta}}| = M^{1/2} (2\pi RT)^{-1/2} \alpha_e 10^{[A-B/(T+C)]} H_v$$

A Gaussian profile is assumed for the laser as an approximation.

For a Gaussian laser of power P_T ,

$$|\bar{F}_L| = \frac{P_T}{2\pi\sigma^2} e^{-r^2/2\sigma^2}$$

where r = distance from spot center. In the approximation where the spot is small compared to the asteroid, the equation becomes

$$\bar{F}_L = \frac{-P_T}{2\pi\sigma^2} e^{-r^3/2r^2} \hat{n}$$

In the dynamic case, it is possible to solve for transient heat flow by solving the following heat flow equation:

$$\begin{aligned} \nabla \cdot (K\nabla T) + \frac{d}{dT}(\rho c_v T) &= 0 \\ K\nabla^2 T + \rho c_v \frac{dT}{dt} &= 0 \end{aligned}$$

In the last equation, it is assumed that k_T (the thermal conductivity) is independent of position and ρ , c_v are time independent. In the full 3D time-dependent solution, all of the above conditions are invoked, and the equations are solved simultaneously using a 3D numeric solver (COMSOL in this case).

In the 2D steady-state solutions, the thermal conductivity is assumed to be small (this is shown in 3D simulations to be a valid assumption as well as from first-principle calculations), and a combination of radiation and mass ejection (phase change) is used:

$$|\bar{F}_L| = |\bar{F}_{\text{rad}}| + |\bar{F}_{\text{Ejecta}}| = F_T$$

$$F_T = \sigma T^4 + M^{1/2} (2\pi RT)^{1/2} 10^{[A-B/(T+C)]} H_V$$

Inversion is not analytically possible, so numerical inversion is used to get $T(F_T)$ which gives $P_v(F_T)$, $\Gamma_e(F_T)$, etc.

In this inversion, a function fit is found for each relevant compound (to 10th order typically):

$$T = \sum_{n=1}^N a_n (\log F_T)^n.$$

A Gaussian approximation to the laser profile is used (this is not critical) to get $T(r)$, $P_v(r)$, $\Gamma_e(r)$, where r is the distance from the center of the spot.

Since radiation goes as the fourth power of T , while the mass ejection from evaporation is exponentially in T , at low flux levels, the outward flow is completely dominated by radiation (you heat the asteroid slightly and it radiates). As the spot flux level increases (spot size shrinks or power increases or both), evaporation (mass ejection) becomes increasingly dominant, and eventually at about $T \sim 2,000\text{--}3,000$ K or fluxes of $10^6\text{--}10^7$ W/m², mass ejection by evaporation becomes the dominant outward power flow and (just as water boiling on a stove) the temperature \sim stabilizes and increasing flux only increases the rate of mass ejection with small increases in temperature. To help illustrate this, the relationship between flux and temperature in the purely radiation-dominated mode is depicted in Fig. 9.

Results from the three methods are briefly summarized below:

- 1D – energetics alone. Use heat of vaporization and set spot flux to $T \sim 6,000$ K. No radiation or conduction included.
- 2D – model elements and compound vapor pressure versus T . Include radiation emission. Ignore thermal conduction.
- 3D – full 3D FEA. Include phase change, vapor pressure, mass ejection, radiation, and thermal conduction.

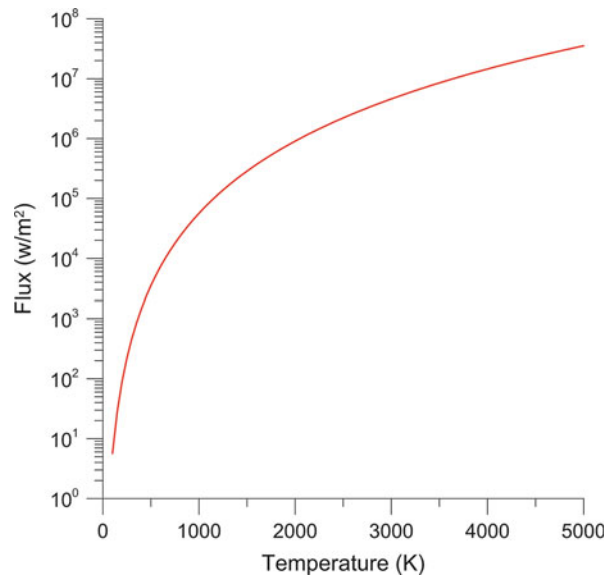


Fig. 9 Relationship between flux and temperature in spot in the radiation-dominated case. In reality the temperature rarely gets above 3,000 K as the power is diverted from radiation to mass ejection

Table 1 List of thermophysical properties of common high-temperature asteroid compounds

Material	H_f (kJ/mol)	H_v (kJ/mol)	M (g/mol)	H_v (10^6 J/kg)	C_v (J/kg-K)	V_{eff} (km/s)	T_{eff} (10^4 K)
SiO ₂	9.0	143	60.1	2.38	730	1.54	0.573
Al ₂ O ₃	14.2	293	102.0	2.87	930	1.69	1.15
MgO	77.4	331	40.3	8.21	1,030	2.87	1.32
ZnS	38.0	320	97.5	2.46	472	1.57	1.28

Here H_f is the heat of fusion and H_v is the heat of vaporization. Effective ejection speed $V_{eff} = (H_v(\text{J/kg}))^{1/2}$ and $T_{eff} = (M^*H_v)/3R$ where $R = k*N_A \sim 8.31$

1D – Energetics Alone: The heat of vaporization of a compound is the energy (per mole or per kg) to remove it from the bulk. Removal energy is related to an effective speed and an effective temperature which are related to but somewhat different than the physical speed of ejection and the physical temperature of vaporization. To be more precise, the term evaporation refers to molecules or atoms escaping from the material (e.g., water evaporating), while boiling is the point at which the vapor pressure equals or exceeds the ambient pressure. At any nonzero temperature, there is a probability of escape from the surface, so evaporation happens at all temperatures and hence vapor pressure is a quantitative measure of the rate of evaporation. The heat of vaporization is also temperature and pressure dependent to some extent. Table 1 gives thermal properties for various materials in asteroids. Figure 9 shows a plot of vapor pressure versus T and flux. These materials have relatively high effective temperatures reflecting the fact that there is a probability distribution of energies and that the increase in vapor pressure versus T in Fig. 9 shows that the thermal probability distribution has a “tail” allowing for escape from the surface at lower temperatures that one would naively conclude from a mean analysis only. A similar analogy is the Saha equation that relates the ionization fraction versus temperature where a mean analysis would conclude that extremely high temperatures are required to ionize an atom, but in fact significant ionization occurs at much lower temperatures due to the probability distribution tails. If power P_T from the laser impinges on the

asteroid in a small enough spot to heat to above the radiation-dominated point (typically 2,000–3,000 K for “rocky” asteroids (vs. 300–500 K for comets)), it is possible to compute the evaporation flux (mass ejection rate) as:

$$\Gamma_e = P_T / H_{eff} \text{ where } H_{eff} = H_v + H_f + \int_{T_a}^{T_v} C_v dT$$

H_{eff} is the energy required (for 1 kg) to raise the temperature to the vaporization point and to vaporize it and includes the heat of vaporization, heat of fusion and energy required to raise the temperature to the vaporization point from the ambient asteroid temperature. T_v is the temperature at which vaporization is occurring and T_a is the initial asteroid temperature. In general C_v (specific heat) is temperature dependent. For most materials $H_f \ll H_v$ and the integrated specific heat $\int_{T_a}^{T_v} C_v dT$ is a small correction (ie $< H_v$). Γ_e is the maximum possible rate of mass ejection. It is possible to get quite close to this maximum if the system is designed properly. In general it is a good approximation to simply use $H_{eff} = H_v$.

2D Thermal Calculation: As mentioned above in this calculation, assumptions are that the thermal conduction is small compared to radiation and mass ejection (a good assumption for most asteroids). Using the equations above and the numerical inversions, it is possible to solve for the temperature distribution and thus the mass ejection and thrust on the asteroid among many other parameters. A summary is shown in Fig. 10 for SiO_2 . The parameter σ (sigma) in the Gaussian beam profile is allowed to vary to show the effects of nonideal beam formation as well as beam and

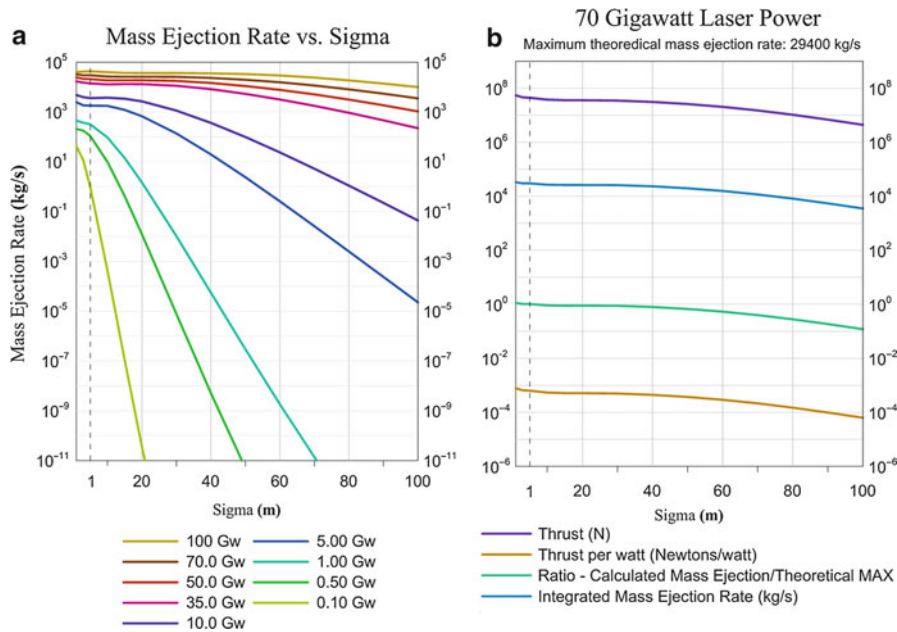


Fig. 10 (a) Mass ejection rate versus sigma (in the assumed Gaussian laser beam profile) for various power levels for the compound SiO_2 . While this is done for a target at 1 AU, it is independent of distance. Note that at the higher power levels, the system is much more tolerant to errors that increase sigma. (b) Thrust, thrust per watt, ratio of integrated total mass ejection to maximum theoretical, and integrated mass ejection versus sigma for a DE-STAR with the target at 1 AU. Nominal diffraction-limited sigma is 5 m, but it is clear there is a very wide latitude (more than 10 \times) to absorb various errors that increase the effective sigma (beam formation, phase noise, beam jitter, and pointing jitter)

pointing jitter. The diffraction-limited σ at 1 AU should be about 5 m. As can be seen, the system is quite tolerant to errors in beam formation, focus, beam bitter, and pointing errors even beyond 10σ as long as the power is high enough. The requirements on a low-power system at equivalent distances are more severe. These relationships also show that it is possible to nearly achieve the theoretical maximum mass ejection rate. Also, note the thrust (N) per watt is close to 0.001 N/W. This is comparable to the Shuttle SRB (solid rocket booster) in thrust per watt. This is not really surprising if you think of conventional propellants as being approximately thermal in nature with temperatures close to the maximum sustainable in the combustion chamber and exhaust nozzle (i.e., a few $\times 10^3$ K).

Asteroid Plume Thrust: The ejecta speed from the asteroid is also close to that of a conventional rocket (a few km/s). The Shuttle SRB, for reference, has a power of about 13 GW and a thrust of about 14 MN and exhaust speed of around 2.6 km/s. The computed thrust for a DE-STAR 4 with 70 GW on target is about the same (thrust) as the SRB assuming an “exhaust nozzle” on the asteroid is nearly isotropic in the forward 2π . This “plume thrust” is what is responsible for the dramatic orbital diversion that is possible with the DE-STAR system. In a **power-limited** system, the thrust per watt is $1/v_{\text{rel}}$, where v_{rel} is the exhaust velocity. Thus a “photon rocket” or photon-propelled system (one of the many other uses of the DE-STAR system is pushing a spacecraft via photon pressure) is the **least efficient** method (in terms of thrust/W), BUT in a **mass-limited** system where mass is being ejected for propulsion (such as in a conventional rocket or an ion engine), the thrust to mass rate (dm/dt) is v_{rel} ($=c$ in relativistic limit) and hence photons are the **most efficient (in terms of thrust/dm/dt)**. This is one of the basic rationales behind ion engines. They can achieve much higher (nonthermal equilibrium) exhaust speeds (typically $10\times$ or more) than a conventional propellant that is largely in thermal equilibrium. There have been proposals to use solar sails attached to asteroids as well as ion engines. Solar sails only have F (thrust) $= 2P/c$, where P is the power intercepted from the Sun on the reflector. The factor of 2 is for perfect reflection. This is used later for a DE-STAR standoff “photon rail gun” propulsion system (Bible et al. 2013). The thrust per watt in this case is $F/P = 2/c \sim 6.6$ nN/W or more than 10^5 times lower than the estimated plume thrust. Current state-of-the-art ion engines (e.g., VASMIR VX-200) use 200 kW and produce 5.7 N with an exhaust speed of 50 km/s ($10\times$ Shuttle main engine H_2 - O_2 and $20\times$ that of the SRB which is ~ 2.6 km/s) and 72 % efficiency using argon and a plasma exhaust equivalent $T \sim 10^6$ K with a thrust per watt of 2.85×10^{-5} N/W or about 3 % of the SRB thrust/W. This is consistent with the exhaust being about 20 times higher speed than the SRB, and hence it should be 20 times less efficient ($5\% \times 0.72$ (eff) $\sim 3.6\%$) in terms of thrust per watt. Of course, the major advantage of an ion engine compared to a conventional propellant is that it uses *much* less propellant for an equivalent impulse (thrust * time), being about 20 times less, and it can be throttled on and off easily. In the case of orbital modification of an asteroid, using the asteroid itself as the propellant is proposed and using a high-power laser driven by solar PV if attachment to the asteroid is desired. This is a modified variant of the DE-STAR system. This is a much simpler and lower-mass system compared to an ion engine (which is quite massive) with extremely long life. In theory the power required to get the same thrust as the VASMIR would be about 10–30 times less with this approach, but this needs to be further verified in lab testing. The plots in Figs. 10 and 11 show the various parameters that come from the 2D analysis.

Interaction Simulations: Figure 11 shows calculations for various expected properties. This is done for SiO_2 , but the results are similar for the other compounds which have been simulated. The vapor pressure and mass ejection and thrust have a roughly exponential rise with temperature, but when computed versus target flux, they enter a nearly linear regime above about 10^6 – 10^7 W/m². This is expected when the dominant flux is due to mass ejection and the vapor pressure, mass ejection

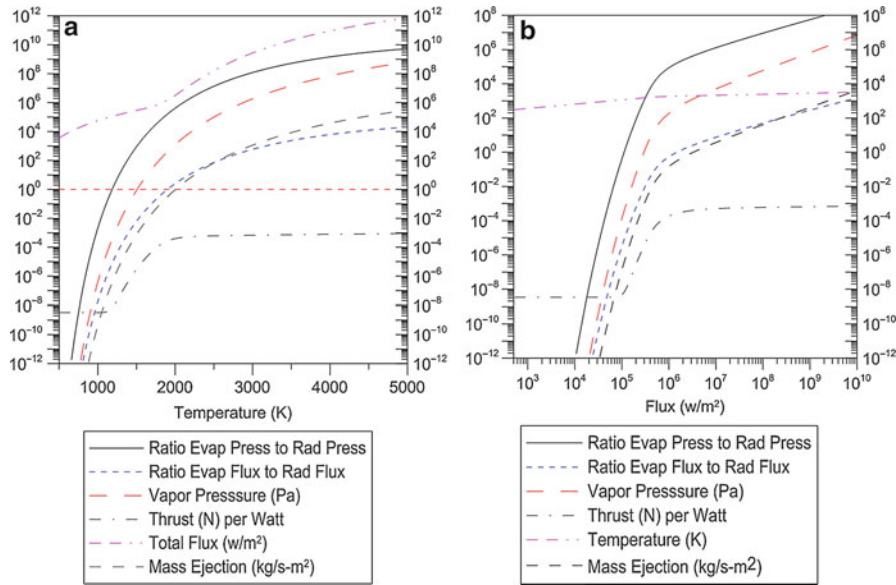


Fig. 11 (a) Simulations of SiO₂ properties versus temperature. (b) Simulations of SiO₂ properties versus flux

rate, and thrust are all approximately linear with power above this point. This is the point above which the desired flux should be. The surface temperature does not change much in this regime just as a pot of boiling water remains at about 100 °C at sea level independent of how high you turn up the flame. This is the same linear regime. Notice the thrust starts at the photon thrust (absorbed in this case) of about 3.3 nN/W and rises more than five orders of magnitude to about 0.1–1 mN/W in the linear regime mentioned above. This value then essentially remains constant at high flux, until extremely high values are reached and ionization begins.

3D Thermal Calculations

In the 3D simulations, all of the above approaches are used, as shown in the thermal transport equations, which must be solved numerically for the temperature distribution. In the model, radiation, mass ejection and phase change, and thermal conduction are included, as well as solutions for both the transient and steady-state cases. This was done with a 3D solver modified to add mass ejection (phase change) for arbitrary materials.

Thermal Conduction: Unfortunately it is not possible to bring asteroids into the laboratory to study their thermal properties, so the desired properties must be inferred from astronomical observations, primarily in the infrared to deduce their properties combined with assumptions about their formation and likely structure. Mueller (2007), Mueller et al. (2007), Harris (1998), and Delbò et al. (2007), among many others, have done excellent work in this area. One can derive the thermal properties by studying the time-varying temperature as deduced from infrared observations. In this way the “thermal inertia Γ (J/m²-K-s^{1/2})” and thermal conductivity K (W/m-K) are derived. The relationship between them is

$$\text{Thermal Intertia } (\Gamma) - \left(\text{J/m}^2 - \text{K} - \text{s}^{1/2} \right) \text{ and Thermal conductivity : } (k_T) - (\text{W/m-K})$$

$$\text{where } \Gamma = (\rho k_T C)^{1/2}$$

$$\rho = \text{density (kg/m}^3\text{)}$$

$$C = \text{heat capacity (J/kg-K)}$$

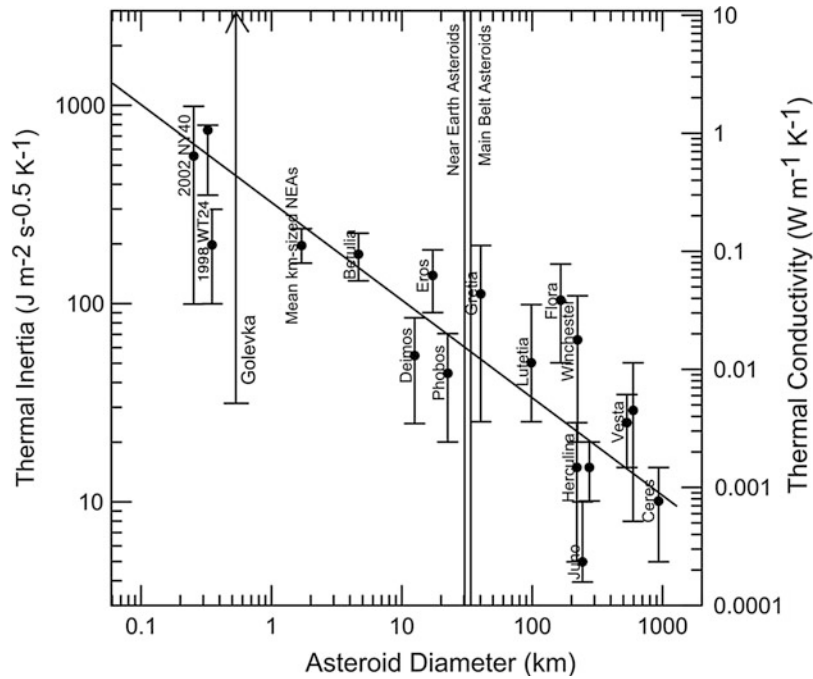


Fig. 12 Thermal properties measured for various asteroids from Delbò et al. (2007)

Hence,

$$k_T = \Gamma^2 / (\rho C)$$

The data shown in Fig. 12 is best fit to the data from Delbò et al. (2007), where D is the asteroid diameter in km:

$$\Gamma = d * D^{-\xi} \text{ with } d = 300 \text{ (km) and } \xi = 0.4$$

$$k_T = 3 \times 10^4 * D^{-0.8} / (\rho C)$$

The trend (with significant variability) is toward smaller asteroids having larger thermal conductivity and larger asteroids having smaller thermal conductivity. Some of this trend may be the “rubble pile” effect for larger asteroids. Thermal conductivity values are important features of the thermal models; a relatively conservative case of $k_T = 1 \text{ W/m-K}$ can be assumed. To put this in perspective, some values for common materials are listed in Table 2.

Rotating Asteroids: Asteroids do rotate but generally quite slowly. A complete picture of rotation properties is not available, but from the limited data on the rotation of larger bodies and the breakup speed, it is estimated that asteroids in the 0.1–1 km class typically rotate no faster than once per several hours. A distribution of measured asteroid rotation rates is shown in Fig. 13.

Results of detailed simulation indicate the rotation properties for more than 6,000 significantly rotating asteroids and conclude that rotation is not an issue in general as larger asteroids (>150 m) are largely gravitational-bound “rubble piles” and for these the maximum rotation is independent of diameter and only depends on density ρ with an angular speed ω and rotation period τ given by

Table 2 Common material thermal properties for comparison to the asteroid thermal properties in Fig. 12

Material	K (W/m-K)	ρ (kg/m ³)	C (J/kg-K)	Γ (J/m ² -K-s ^{1/2})
Nickel	91	8,850	448	19,000
Iron	81	7,860	452	17,000
Granite	2.9	2,750	890	2,600
Ice (solid)	2.3	917	2,000	2,040
SiO ₂ (solid)	1.04 (200 °C)	2,200	1,000	1,510
Water (liq 0 C)	0.56	1,000	4,200	1,500
Snow (firm)	0.46	560	2,100	740
Soil (sandy)	0.27	1,650	800	600
Pumice	0.15	800	900 (varies significantly)	330
Styrofoam	0.03	50	1,500	47
Air	0.026	1.2	1,000	5.6
Moon (regolith)	0.0029	1,400	640	51

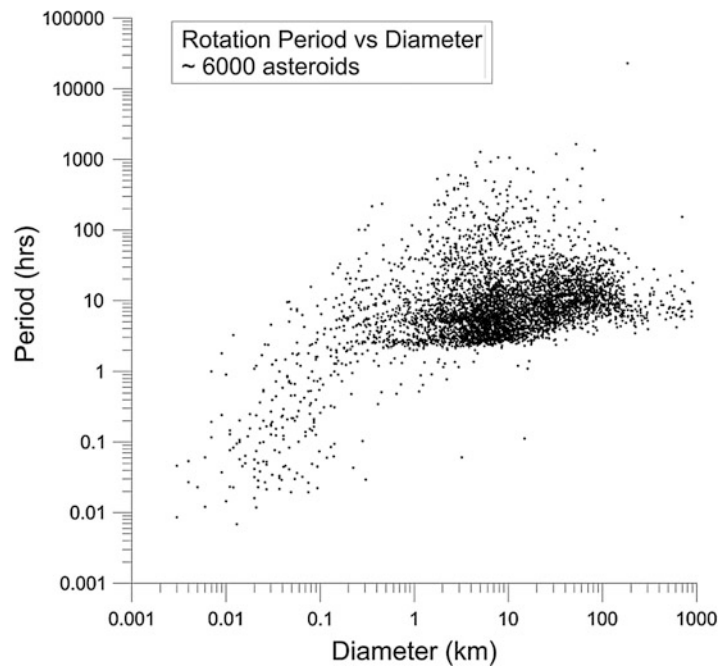


Fig. 13 Measured rotation period of 6,000 asteroids. Notice the very sharp cutoff at just above 2 h for larger diameter asteroids (Data from Minor Planet Center. Warner et al. (2009))

$$\omega = \sqrt{\frac{4}{3}\pi G\rho} = \frac{2\pi}{\tau}, \tau = \sqrt{\frac{3\pi}{G\rho}}$$

$\tau \approx 1.19 \times 10^4 \rho(\text{g/cc})^{-1/2} \text{s} \approx 3.3\rho^{-1/2} \text{h}$ – this is independent of diameter.

As an example, assuming a typical average density of 2 g/cc gives $\rho = 2 \rightarrow \tau = 2.3 \text{ h}$. There is indeed a remarkably sharp cutoff in rotation periods very close to 2 h (about 10 rotations per day) for asteroids greater than diameters of approximately 150 m. Some smaller asteroids can rotate faster as they can have a tighter binding than purely gravitational (such as an iron meteorite), but these are

relatively rare and even the fastest ones can be dealt with since the mass ejection begins so quickly (type < 1 s) after the laser is turned on. As is seen in the transient thermal simulations below, the mass ejection and hence thrust begin within about 1 s for a DE-STAR 4 at 1 AU. It is largely a flux issue so that for the same flux at any distance, the mass ejection remains at this rate. This is assuming solid SiO_2 which is extremely conservative. Loss is included to mimic the absorption qualities of asteroids which are very absorptive having typical reflection coefficients around 5 %. Thus a rotating asteroid with this rate (1 h) poses little problem. More interesting perhaps would be an attempt to spin up (or down) an asteroid depending on beam placement.

3D Results: Hundreds of 3D model simulations have been run, and a few salient results are apparent. Perhaps the most interesting bottom line is that starting with the simplest assumptions, namely, energetics only and conservation spot flux were borne out as being valid, but more sophisticated tools are available with which to analyze and optimize the system.

4D Simulations: For the case of dynamic targeting and rotating objects, time evolution has been added to the 3D solver (Johansson et al. 2014). Some of this is motivated by the need to understand the time evolution of the mass ejection under dynamic situations. This is partially shown in Fig. 14 (right) where the time evolution of the temperature at the center of the spot is shown. It is now

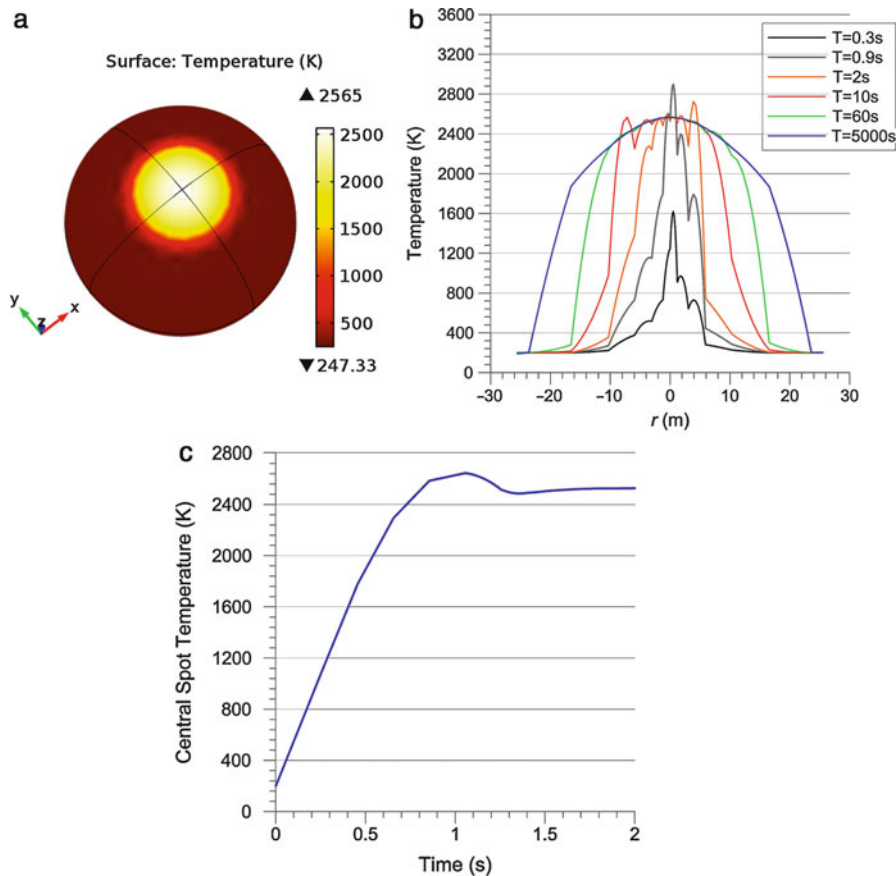


Fig. 14 All cases refer to SiO_2 as the equivalent material. (a) Steady-state surface temperature distribution for a 100 m diameter asteroid at 1 AU with a DE-STAR 4 Gaussian beam derated to 50 GW. Spot diameter is approximately 30 m. Temperatures rise to the point of being mass ejection limited, which is about 2,600 K in the center of the spot. Solar illumination is modeled with an isotropic average of 350 W/m^2 . (b) Temperature distribution versus theta (angle from beam axis). High-frequency substructure is due to numerical meshing. (c) Transient time solution of temperature in the spot center (K) versus time (seconds) after the laser is turned on at $t = 0$. Initial temperature is 200 K. Mass ejection begins within 1 s

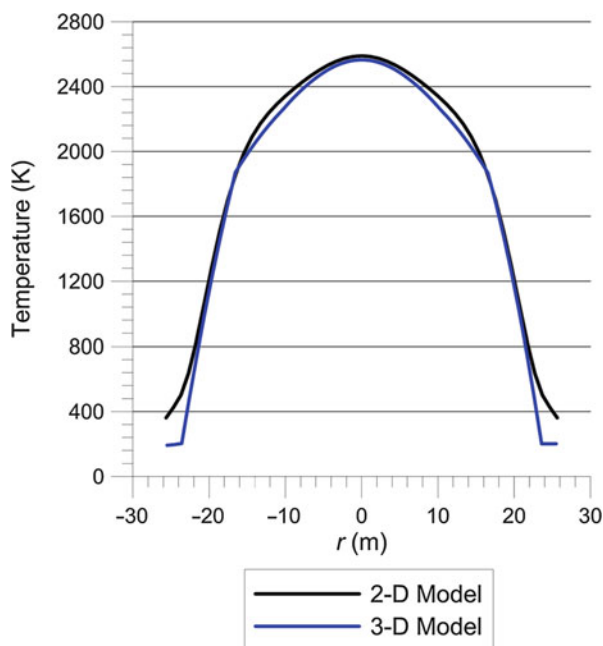


Fig. 15 Comparison of 2D and 3D models: temperature versus theta (angle from beam axis on sphere) for SiO₂ with 50 GW total power and sigma = 5 m Gaussian beam illumination. Results are nearly identical in the critical central region

possible to simulate full dynamics and apply this to the case of rotating asteroids. The same techniques can be applied to pointing jitter and “laser machining of the asteroid or other target.”

Comparison of 2D and 3D Simulations: While the 3D simulations give time transient solutions and include full thermal conduction, they lack the numerical flexibility of the 2D solutions. Results of the temperature distributions for a Gaussian laser illumination are compared and found to be very close in their predictions. This builds confidence that it is possible to do both 2D and 3D simulations with high fidelity. The ultimate test will come when comparing model results with laboratory tests. Figure 15 compares the temperature distribution for a 3D model (blue) with a 2D model (black). They have nearly identical results in the critical center of the spot and then differ in the wings. As laboratory tests are refined, the results will feed back into the models.

Orbital Diversion via Plume Thrust

In general, it is not necessary to evaporate the asteroid to avoid an impact scenario. It is sufficient to change its orbit enough to miss the Earth. The ability to stand off and divert using the plume thrust that DE-STAR generates is an extremely attractive approach. Consider the example of Apophis. It is approximately 325 m in diameter with a mass of 4×10^{10} kg and has an orbital speed of 30.7 km/s with a 30 h rotation. A direct hit would have a yield approaching 1 GT (gigaton TNT). This would be a bad day. The momentum is approximately $p = mv \sim 1.2 \times 10^{15}$ N-sec. If a theoretical thrust to power ratio of 1 mN/W can be achieved, then the thrust with a DE-STAR 4 would be 7×10^7 N. If it is possible to activate DE-STAR for 1 month, then a change in momentum of Apophis of $\delta p \sim 1.7 \times 10^{14}$ N-s is possible. The effect on the orbit depends on the details of when and where the interaction begins, but it is possible to estimate the deflection angle to be $\delta\theta \sim \delta v/v = \delta p/p \sim 0.14$ radians or a $\delta v \sim 0.14v \sim 4.2$ km/s. This is enormous by standards the deflection community speaks of. A simplistic distance deflection is given by δr (miss distance) $\sim L \delta\theta$ ($L = 1$ AU 1.5×10^{11} m) $\sim 2 \times 10^{10}$ m $\sim 3,000 \times$ Earth radii. This is 50 times the Earth-Moon distance. This is obviously extremely

conservative and less extreme scenarios are possible. In addition when running actual orbital trajectories as shown below the simple calculation shown above is often pessimistic and the actual orbital modification can be much larger for the same thrust since the asteroid is in a gravitational bound orbit relative to the Earth's orbit. See section on "DE-STARLITE" for a detailed example of this. The amplification factor is typically a factor of three times the naïve deflection calculation depending on the details of the asteroids orbit. Keyhole amplifications due to the earth-moon orbit are also very large.

Targeting and LIDAR Mode: One of the difficulties with asteroid mitigation in general is knowing where the targets are. Generally asteroids are found by looking for them in the visible bands using their reflected sunlight or in the thermal IR using their heat signature or with radar. It is possible to use a DE-STAR system for active illumination of targets to aid in both their detection and orbital refinement. This is done in much the same way that a radar system works except the laser beams are much smaller, providing much finer target determination and much greater range. The general technique is sometimes referred to as Light Detection and Ranging (LIDAR). The same phased-array optical system is used for the reception of the return light, as is used for the transmission of the laser. In this case, the system is run in a gated or long-term pulsed mode. The light travel time to 1 AU is about 8 min or a round trip light travel time of 16 min. The laser could be turned on to scan potential targets and then turned off just before the photons that are scattered off the target are expected to return and switch to a receive mode. This then forms a complete LIDAR system with the same optics used for transmit and receive. The receive system could also be phased to form a full phased-array receiver or could be run in a mode where each element acts as an independent receiver with the sum of all sub-elements co-added before detection. There are advantages to this mode in both simplicity of operation and in that a much larger field of view is received eliminating scanning the field for reception. The disadvantage is the increased background from a larger field of view per sub-element.

The return signal is computed for a variety of mission scenarios, as well as the equivalent mapping times for small error boxes to full sky blind surveys. Illustrated in Fig. 16 are the background levels relevant for survey times at the target illumination (the same as the mitigation) wavelength of 1 μm . The relevant backgrounds are the cosmic infrared background (CIB) and the zodiacal backgrounds, which include both scattered sunlight and thermal emission. This technique not only allows for an "in situ" and "co-aligned" determination of the target position but also gives ranging from time of flight (or phase modulation) as well as speed from measured Doppler. Here a heterodyne technique is assumed for detection, which is now feasible with at the baseline wavelength. This is another relatively new development in photonic technology.

Backgrounds for Remote Targeting: In order to determine the signal to noise of the return signature, it is necessary to understand the nontargeting signal-related sources of photons. This is generically referred to as the background. There are a number of such backgrounds that are important. Going outward from the detector to the target and beyond, there are:

- Dark current and "readout noise" associated with the detector.
- Thermally generated photons in the optical system. It is assumed the optical system is mostly running near 300 K.
- Solar system dust that both scatters sunlight and emits from its thermal signature. Dust in the solar system is typically at a temperature of about 200 K. This is generically called "zodiacal" scattering and emission, respectively, or "zodiacal light" or zodi for short.
- Photon statistics noise from the laser hitting the target. This is due to both the counting statistics nature of the light and its detection and to its bosonic nature (spin 1 statistics).

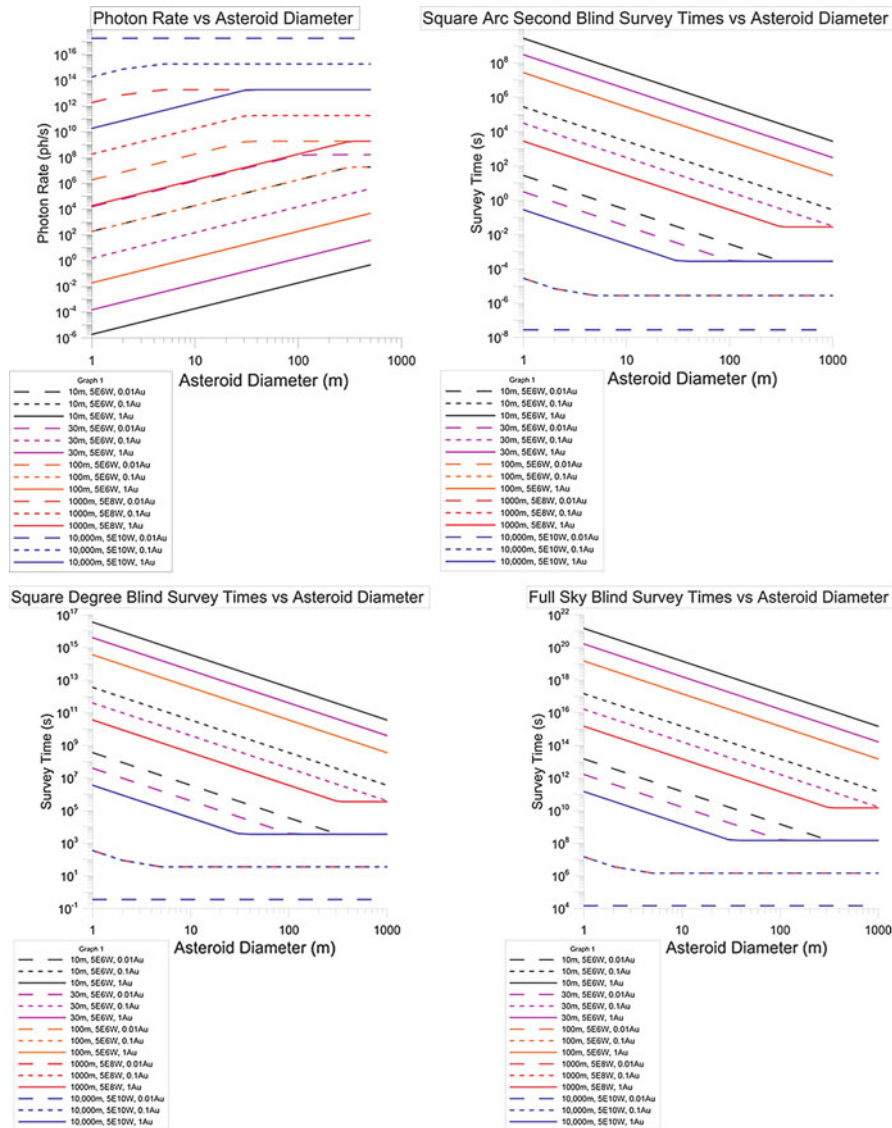


Fig. 16 Active illumination (LIDAR mode) scenarios showing photon return rate versus asteroid diameter and system parameters as well as blind survey integration time to detect target versus sky fraction searched, asteroid size, and system parameters (Riley et al. 2015)

- Scattering of sunlight from the target itself as it is illuminated by the Sun.
- Thermal emission of the target.
- Distant background stars that are in the field of view.
- Sunlight scattered into the field of view for targets that are near to the Sun in the field of view. This is generally only important for targets that are very close to the Sun along the line of sight, though off-axis response of the optical system can be an issue as well.
- The far-IR background of the universe is known as the cosmic infrared background or CIB. This is the total sum of all galaxies (both seen and unseen) in the field of view in the laser band that are NOT blocked by the target. This is relevant IF the target is smaller than the receive beam. It is not relevant to first order IF the target is larger than the receive beam (or spot at the target distance).
- The cosmic background radiation or remnant radiation from the early universe. This turns out to be negligible for laser-directed energy systems.

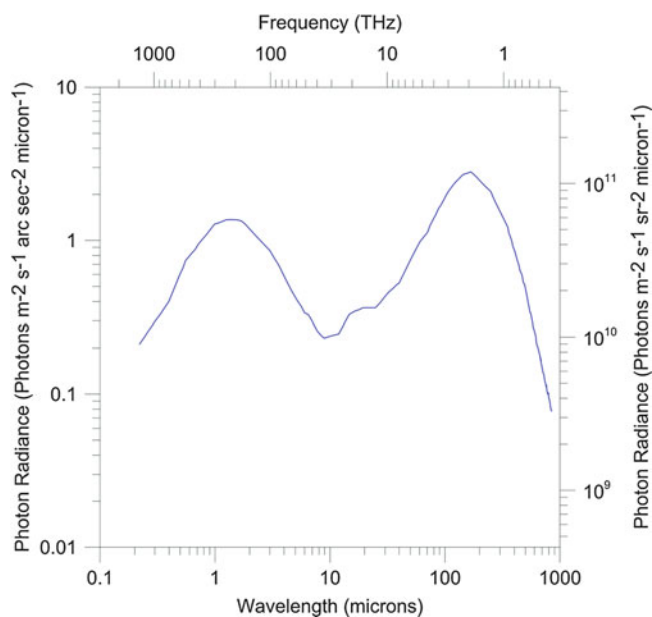


Fig. 17 Diffuse CIB component flux versus wavelength

In all of these cases, the fact that the laser linewidth (bandwidth) is extremely narrow (from kHz to GHz depending on the system design) and the field of view is extremely narrow mitigates these effects which would otherwise be overwhelming for a broadband photometric band survey. Heterodyning is possible at 1 μm and will greatly aid in detection.

Cosmic IR Background: The CIB was first detected by the Diffuse IR Background Explorer (DIRBE) instrument on the Cosmic Background Explorer (COBE) satellite launched in 1989. It is an extremely faint background now thought to be due to the sum of all galaxies in the universe from both the stellar (fusion) component at short wavelengths near 1 μm and from the reradiated dust component near 100 μm . On large angular scales (degrees), it is largely isotropic though at very small angular scales (arcsec), individual sources can be detected. The diffuse CIB component is shown in Fig. 17.

Zodiacal Light: Like the CIB, the zodiacal light has two components and both involve dust in the solar system and the Sun. The sunlight both scatters off the interplanetary dust grains giving a “streetlight in fog” effect and heats the dust grains which then reradiate in the mid- to far IR. The scattered component can be seen with the unaided eye in dark extreme latitudes and is sometimes known as the “Gegenschein” and traces the ecliptic plane. The dust grains are in rough equilibrium through heating by the Sun and cooling through their own radiation. This “background” is NOT isotropic but is highly anisotropic depending on the position and orientation of the observer in the ecliptic. This was studied in detail by the DIRBE instrument on COBE. As seen in Fig. 18, based on some of the DIRBE measurements, the brightness of both the scattered and emitted components varies dramatically with the observed line of sight relative to the ecliptic plane. In the plot the angle relative to the ecliptic plane is given by the ecliptic latitude (Elat) where $\text{Elat} = 0$ is looking in the plane and $\text{Elat} = 90$ is looking perpendicular. The situation is even more complex as the scattered and emitted components vary with the Earth’s position in its orbit around the Sun. By comparing the CIB and the zodi, it is clear that even in the best lines of sight (perpendicular to the ecliptic plane), the zodiacal light completely dominates over the CIB. For the JWST mission, the zodi light is typically the limiting factor for IR observations. When observing asteroids with active illumination (LIDAR mode), the zodi is also an important factor. However, since illumination occurs with an extremely

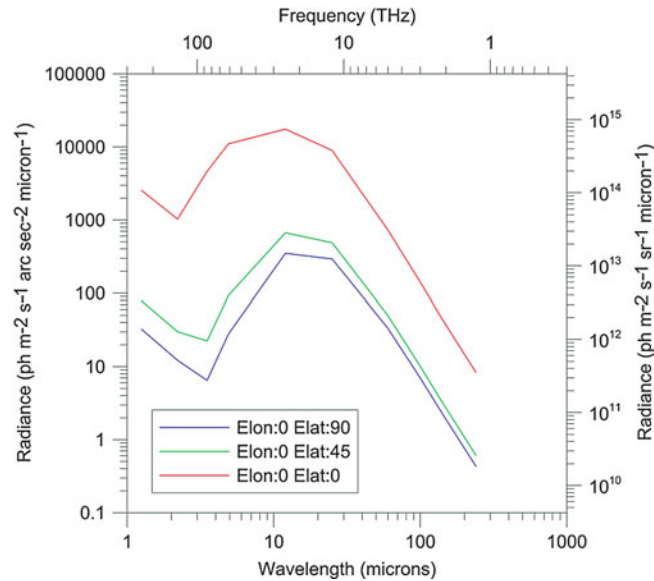


Fig. 18 Zodi background flux versus wavelength

narrow laser bandwidth, and detection occurs with an extremely matched narrow bandwidth, it is possible to largely reduce the zodi and the CIB to negligible levels. This is NOT necessarily true in broadband photometric (typically 30 % bandwidth) surveys that search for asteroids using scattered sunlight or using the thermal IR signature of the asteroid. This is one significant advantage of active illumination. The baseline laser amplifiers can be run with bandwidths between less than 100 Hz and 10+ GHz. The advantage of smaller bandwidths is the larger coherence length and stability, while the advantage of the larger bandwidth is higher power levels when in a stimulated Brillouin scattering (SBS)-limited mode. The current generation of high power density (1–3 kW) Yb fiber amplifiers uses large bandwidth (typ ~10 GHz) in order to mitigate the SBS limit by broadening the bandwidth, while the lower-power units (few hundred watts) have intrinsic bandwidths that are much less (typ ~100 Hz). There is a path forward to high power and lower bandwidth that is preferred for DE-STAR. To compare to the CIB and zodi backgrounds, Figs. 18 and 19 show the wavelength bandwidth in μm versus the frequency bandwidth in Hz.

Optical Emission: Since the plan is to use the same phased-array elements used to transmit the optical emission of the laser illuminator, it is necessary to compute the optical emission rate into the detector. The optics are assumed to be at roughly 300 K for simplicity (this could be changed in some scenarios), indicating a brightness or emission rate of about $1.1 \times 10^7 \gamma/\text{s}\cdot\text{m}^2\cdot\text{st}\cdot\mu\text{m}$ for unity emissivity (or for a blackbody emitter) at $1.06 \mu\text{m}$. This is clearly an overestimate but represents a worst case. Under the assumption of a diffraction-limited system, the etendue of the optics is such that $A \Omega = \lambda^2 \sim 10^{-12} \text{m}^2\cdot\text{st}$. The bandwidth of reception must also be included. Here a matched filter spectrometer is assumed (to get Doppler) with a bandwidth equal to the laser linewidth. As explained above, this is typically $10^4\text{--}10^{10}$ Hz or approximately 4×10^{-11} to $4 \times 10^{-5} \mu\text{m}$. The total per sub-element is thus an emission of about 4×10^{-16} to $4 \times 10^{-10} \gamma/\text{s}$ again for an emissivity of 1. This is an extremely small rate compared to the return LIDAR flux (see Fig. 16). Compare the brightness of $1 \times 10^7 \gamma/\text{s}\cdot\text{m}^2\cdot\text{st}\cdot\mu\text{m}$ for unity emissivity to the CIB and zodiacal light which are both much larger. For comparison, note that when looking directly at the Sun, the brightness of the solar surface is $\sim 5 \times 10^{25} \gamma/\text{s}\cdot\text{m}^2\cdot\text{st}\cdot\mu\text{m}$ at $1.06 \mu\text{m}$. Assuming a diffraction-limited system, the resulting photon rate would be about 2×10^3 to 2×10^9 for laser (receiver) bandwidths from 10^4 to 10^{10} Hz as above. This is NOT small compared to the CIB and zodi (as was the optical thermal emission), but it

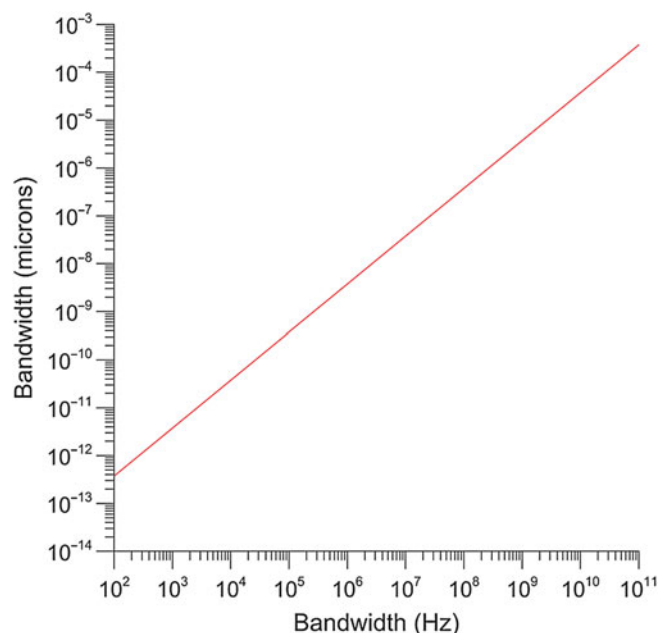


Fig. 19 Laser wavelength bandwidth in μm versus the frequency bandwidth in Hz

is still small compared to the LIDAR photon return rate for a DE-STAR 4 illuminating a 100 m asteroid at 1 AU. It does, however, point out the need to be reasonably careful in rejecting direct solar illumination in the off-axis response.

Ground Versus Airborne Versus Space-Based Systems

While the baseline for DE-STAR is an orbital approach, a ground-based approach offers many obvious advantages in terms of testing and deployment, while the severe impediment of the atmospheric perturbations may be insurmountable for the foreseeable future. In all initial “roadmaps” to DE planetary defense, ground deployment for the smaller systems during test and debugging is a crucial step. The great strides made in adaptive optics for astronomy and situational awareness allow sub-arcsecond beam formation. Based on the active laser guide star programs, micro-radian beam formation is feasible from the ground. The transmission on clear days from excellent ground-based sites allows for less than 10 % transmission loss near 1 μm from ground to space. On cloudy days the transmission will be essentially zero. However, it is not the transmission which is the critical issue. It is the atmospheric turbulence or “seeing” – phase perturbations in the beam formation that is the limiting factor. One great advantage of a phased-array approach is that every aperture element is part of an “adaptive optics system” by the very nature of the phased array. In addition, rather than mechanically adjusting the phase front across a sub-optic in a classical adaptive optic system, DE-STAR will have much higher servo phase control bandwidth. This will lead to greatly improved adaptive optics performance, the limits of which are still to be explored. The early and smaller versions of DE-STAR, such as a DE-STAR 1 (10 m aperture), can be used from the ground to explore not only system design and performance but also may allow for initial space debris mitigation. As illustrated in Fig. 5, the beam size θ (nrad) for an aperture size d (m) system is θ (nrad) $\sim 2 \times 10^3/d$. For reference the “seeing” from an excellent ground-based mountain top site (e.g., Mauna Kea) is about 2 μrad RMS at 1 μm wavelength. Ground-based seeing is typically given in arcsecond where 1 arcsec $\sim 5 \mu\text{rad}$, while adaptive optics are often quotes in wavefront error (often in nm) or in milliarcsec (mas) where 1mas ~ 5 nrad. It is important to note that

seeing is usually much more stable at night due to thermally driven perturbations during the day and that the “seeing” quoted for ground-based systems is for nighttime operation. With adaptive optics and decent Strehl ratios ($\sim > 0.5$), 50 mas or 250 nrad at 1 μm wavelength is expected when using multiple active laser guide stars being planned for the next generation of ELT (extremely large telescopes) such as the TMT (Thirty Meter Telescope) among others when operated at night (of course). This (250 nrad) is approximately the beam size for a DE-STAR 1. Extremely aggressive sites, such as being above the boundary layer at Dome A, may allow even better adaptive optics and would be a possibility for small DE-STAR deployments. The extremely high-speed phase control of DE-STAR may allow even better Strehl ratios. This territory needs to be explored. For systems capable of true planetary defense (DE-STAR 3 or 4), one would need to have 100–1,000 times smaller beams, and thus ground-based deployment, while not impossible to imagine someday, is not likely to be effective with currently understood technologies for atmospheric perturbation mitigation. However, this area should be explored. In order to perform a proper analysis, the issues of weather (cloud cover, and other atmospheric distortions) and day/night seeing would have to be factored in. Daytime adaptive optics is also a complicated issue that needs further study.

Airborne platforms offer the advantages of reduced atmosphere but usually severe operational constraints. Fixed wing aircraft are particularly problematic due to high-speed turbulence and airframe microphonics. Airship- and balloon-borne platforms are another alternative as balloons operate at above 30 km with near-zero relative airspeed. Balloon-borne platforms are viable for the smaller DE-STAR systems for multiple uses, but one of the primary issues is power. Beamed power from the ground is one option that has been studied in some detail for other programs. One could imagine large fleets of airship- or balloon-borne platforms, but it does not seem feasible for all but the smallest systems.

Space-based deployment offers many advantages with the severe disadvantage of launch cost. Much of the current focus is on ultralow areal mass systems with a goal of under 1 kg/m^2 for overall areal density. With the exception of thin film holographic lenses, no current technology can meet this goal. This optical possibility is the subject of active research. The lowest launch energy solution is a LEO Sun synchronous orbit to allow constant (except for eclipses) solar illumination and a relatively constant thermal environment. More stable orbital environments such as at a Lagrange point or possibly at geosynchronous orbits are more costly to achieve and vastly more complex to service. A lunar surface deployment might be another choice but again is much more difficult logistically and much more costly to deploy but could be a future defensive position for the Earth.

Pointing Issues

The pointing requirements of the DE-STAR system are one of the more difficult technical challenges. Ultimately, the requirements for achieving high flux on target drive the overall pointing and thus the sensing and servo feedback loops. Unlike a classic optical system, a phased array offers both advantages and challenges compared to the bulk rigid body requirements of a system like the Hubble Space Telescope. The sub-element sizes of even the largest DE-STAR units are currently baselined to be in the meter diameter class (shroud size limited). Experience with rigid body pointing from the HST and upcoming JWST as well as many other space-based telescopes can be leveraged. As mentioned, HST had a 24 h RMS of 35 nrad. If each sub-element is pointed to this level but with uncorrelated pointing errors to its neighbors (clearly there will be some cross talk), the question is “what will the overall effect be on the synthesized beam?” Simulations of these scenarios are occurring now, and this will be covered in a future optical design paper. Since the beam from a 1 m sub-element (as an example) has a beam size of approximately 2 μrad , the individual element pointing error can be much smaller than the individual element beam size. Correlated pointing errors

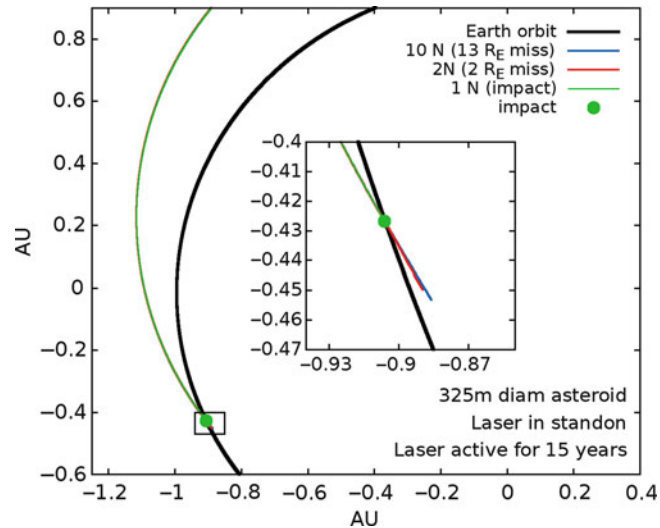


Fig. 20 Orbital deflection versus thrust for an Apophis-class asteroid with a diameter of 325 m and a laser on time of 15 years. Private communication K. Walsh 2014. Note the relatively small amount of thrust needed to deflect the target (2N yields about a 2 Earth radii miss)

are a much more serious issue and one where the overall feedback loop needs to feed information to correct for the final beam pointing. This is a nontrivial problem and one where significant work needs to take place for the largest systems where sub-nanoradian final beams need to be synthesized.

A related effect of phase errors has been simulated extensively. Here the effect is opposite of the effect of pointing errors. For phase errors, complete correlation of the phase errors (or overall shifts) is canceled out to first order since it is the phase **differences** and not the absolute phase that is important. Large-scale correlated phase errors are important however. For example, a linear phase shift across the array would be equivalent to a pointing error. Again, the servo loop must correct and control the phasing to make a phased array.

The effects of random phase error as might arise from phase noise in the amplifiers or high-frequency (beyond the servo bandwidth) mechanical vibrations have also been simulated. A Monte Carlo simulation is used with RMS phase errors of 10^{-3} to 1 wave (2π equivalent phase) and from 2 to 10^4 elements of individual sizes from 0.01 m to beyond 1 m and finds that the initial assumption of maintaining 1/10 wavefront error is a reasonable one, though 1/20 would be significantly better. Results are shown in Fig. 20. Simulation results are compared to simple Ruze theory (which is technically not appropriate due to the assumptions of correlation sizes in Ruze theory). The relationship from D’Addario (2008) is used:

$$\frac{\langle I \rangle}{I_0} = \frac{1 - e^{-\sigma_0^2}}{N} + e^{-\sigma_0^2}$$

where I_0 is the flux with no phase perturbation, $\langle I \rangle$ is the expected value of flux with phase perturbations, σ_0 is the RMS phase perturbation with zero-mean Gaussian distribution, and N is the number of elements. Simulation results agree extremely well with the simple Ruze exponential roll of forward gain or flux on target wherein the limit of infinite number of aperture becomes $I = I_0 e^{-\text{Var}(\varphi)}$, where $\text{Var}(\varphi)$ is the variance of the phase per element, I is the flux on target with phase perturbations, and I_0 is the flux on target with no phase perturbations.

“Stand-on” Applications: DE-STARLITE

While the primary motivation for DE-STAR has been as a “standoff defense” system, it can be used in a variety of modes where much smaller systems can be used as “stand-on” systems. The use of the same system in miniature to get close to a target and then use the focused laser in the same mode but at much closer distances allows for applications where a high flux laser can be used for remote laser machine of targets in asteroid or even lunar or Martian mining as well as for asteroid deflection via the same “plume thrust” mechanism outlined above. An example of this is the DE-STARLITE mission where a small (1–1,000 kW) system is taken near to the asteroid and mass ejection is initiated. The advantage compared to a simple mirror focusing on the asteroid is that the mirror must have an $F\# < 2$ to be effective on high-temperature rocky compounds which requires getting the mirror extremely close to the asteroid (typically 10–100 m away). The reason that the $F\#$ has to be so low, for a mirror, is that the Sun is not a point source and thus the flux on target I_T (W/m^2) is the flux at the surface of the Sun divided by 4 times the $F\#^2$; thus, $I_T = I_{sun}/4 F\#^2$. The flux at the surface of the Sun is about $60 MW/m^2$, and thus with an $F\# = 2$ mirror, the spot flux on the target would be about $4 MW/m^2$ which is just barely enough to start significant evaporation of rocky materials unless there are significant volatiles present. An $F\# = 1$ mirror would be much preferred in this case. This is the same reason that a simple mirror at the Earth will not evaporate distant asteroids unless the mirror diameter is roughly the size of the distance to the target (i.e., 1 AU mirror diameter). While using mirrors close to an asteroid is not insurmountable, the close proximity can cause severe optical pitting and dust buildup on the mirror. DE-STARLITE can stand off some 1–100 km away from the target and does not require Sun-target alignment allowing much more flexible steering. DE-STARLITE can also run pulsed if needed for more flexible mission scenarios. In all of these cases, the asteroid material is converted into its own propellant offering a much more efficient and powerful thruster than an ion engine of equivalent power and needed no propellant other than the asteroid itself.

Studies to date indicate that Apophis-class asteroids (325 m diameter) can be deflected with a dedicated mission using less than 100 kW of power for a mission that gives roughly a decade of active mission time on target. Since the asteroid itself is the “rocket fuel,” such a mission does not suffer from having to take up a very large fuel load as required by an approach that uses ion engines only. A combined mission with ion engines for transport of the laser to the target and use of the ion engines for station keeping looks feasible with the upcoming SLS (Space Launch System). As a specific example, the deflection of a 325 m diameter asteroid (like Apophis) is studied, assuming a DE-STARLITE stand-on mission with the laser on for 15 years with a reasonable Earth-crossing orbit. A force as small as 2 N is sufficient to cause a 2-Earth-radius miss distance. Results of an orbital propagation simulation are shown in Fig. 21. Assuming a 0.1 mN/W (optical), this implies a 20 kW laser would be sufficient. A more conservative approach would use a 100 kW-class laser. In either case this is an extremely efficient approach to the mitigation of large asteroids using lasers. One option currently being studied is to use a laser add-on to the ARM mission concept where ion engines are used to propel the spacecraft to the asteroid and the laser is used to deflect it. This hybrid approach (ion engines + laser) works extremely well. Figure 21 shows the latest design concept for DE-STARLITE with 100 kw of solar PV. Since the build time after warning that an impact is likely, is not trivial, a better approach would be to keep a system (or several) in LEO or GEO or another orbit ready for a threat. This greatly reduces the total time required for mitigation. In the next few figures, we show the current status of the designs for the DE-STARLITE stand-on system. As seen in Fig. 22, the total time for (laser on) deflection for even large targets like Apophis are quite small.

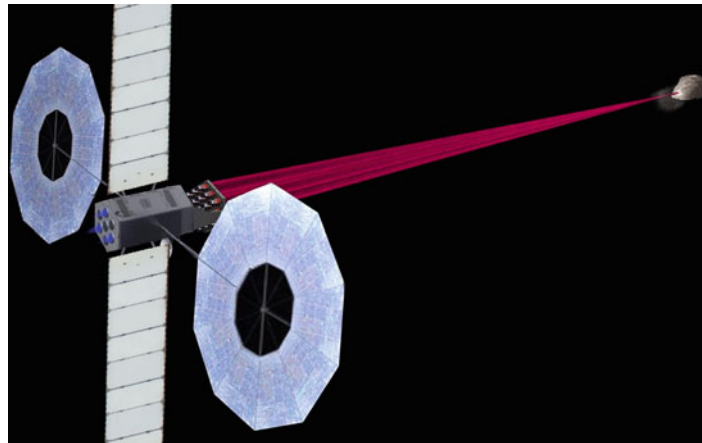


Fig. 21 Artistic rendering of a deployed DE-STARLITE spacecraft deflecting an asteroid (Kosmo et al. 2014). The spacecraft is outfitted with two 15 m diameter ATK MegaFlex PV Arrays that give a total of 100 kw electrical power, a z-folded radiator deployed up and down, a laser array mounted on a gimbal at the front, and ion engines at the back. The laser array can be either a phased array or a parallel non phased array. Larger systems up to a megawatt fit within the SLS Block 1 launch vehicle

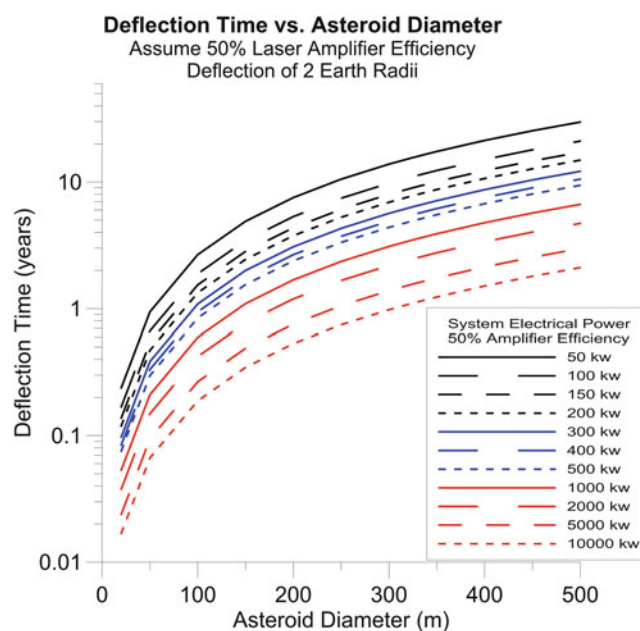


Fig. 22 Laser deflection time needed to achieve 2 Earth radii miss distance vs electrical power available assuming 50% amplifier efficiency and 80 micro-N/w_{opt} coupling efficiency. Note that this is the laser on time not the warning time. The warning time needs to include a build and travel time from LEO to target. The time shown here is the time the laser is actually on. The asteroid density is assumed to be 2000 kg/m³

Laboratory Testing

A laboratory test system was constructed to check calculations and simulations. The test system consisted of 19-fiber CW lasers, each of which was homogenized in an 800 μm core fiber and then reimaged to simulate active phase control. Each fiber had a diameter of about 150 μm and was fed with 2.1 W diode laser at 808 nm. The beam diverges with a NA ~ 0.2 and reconverges with a

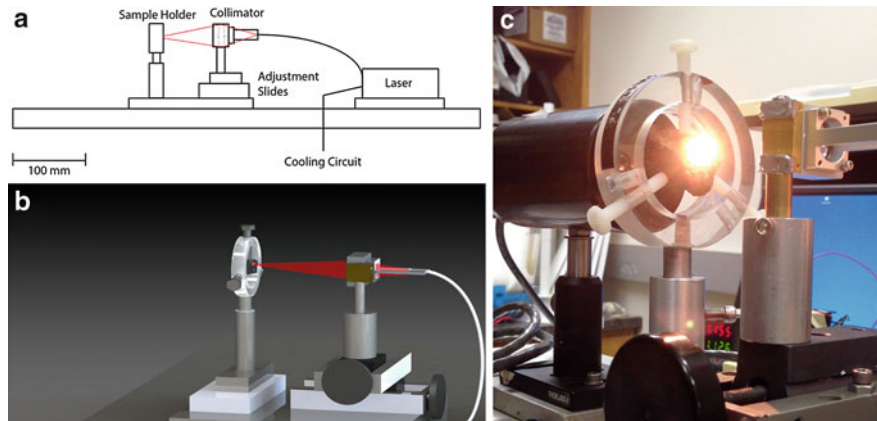


Fig. 23 (a) Cross-sectional diagram showing laser (which is 19 individual fiber-fed lasers) and the re-collimating optics. (b) Rendering showing beam expansion and imaging as well as sample holder. (c) Laser firing at a target (basalt in this case)

roughly 1:1 ratio to produce a spot that was about 1 mm in diameter. Fluxes up to 40 MW/m^2 are achieved which is close to the target of a DE-STAR 4 at 1 AU. For reference, the surface of the Sun (assuming a 5,800 K surface) has a flux of about 60 MW/m^2 . When the laser is fired at a target, an extremely intense white hot spot is created that lights up the room and vaporizes every material tested. So far, tests are done outside the vacuum chamber, but vacuum tests will begin shortly. Diagnostics include IR (out to $12 \mu\text{m}$) and visible light cameras as well as a fiber-fed optical spectrometer. Optical coupling from fiber tip to target was measured at about 90 %. Mass ejection was definitely observed (holes were punched through), but quantitative comparison to mass ejection model will be done in vacuum as the vapor pressure would have to exceed 1 atmosphere for normal evaporation. For basalt, the measured mass ejection (in 1 atm air) was 0.42 mg/s, while the theoretical maximum for this test was 2.2 mg/s. One significant issue is the complex nature of the test materials that are being evaporated. Some standard targets will be used in the vacuum tests. Air convection is also a serious issue, so it is not surprising that the measured mass ejection is less than anticipated for a variety of reasons. Plain sand from the local beach was used as a target; the sand was placed in a small crucible and the laser energy melted it into a glass ball as well as vaporized some of it. The laboratory setup and associated simulation results are shown in Figs. 23 and 24.

Standoff Approach for Efficient and Cost-Effective Impact Risk Mitigation

There is a fundamental difference between DE-STAR and previously described approaches to orbit deflection. All currently described concepts are “stand-on” systems, in that assets required for orbit alteration would need to be deployed onto, or at least very near, the threatening asteroid. DE-STAR is a standoff system that would be capable of altering an asteroid or comet’s orbit from afar. Costs associated with DE-STAR development would be amortized over multiple threats and over multiple applications beyond planetary defense, since a functioning system could be used repeatedly. Asteroid 2012 DA14 (~45 m) was discovered 1 year before its close approach; could a kinetic impact mission have been attempted, had the asteroid been on a collision course? If the object that struck near Chelyabinsk had been discovered 1 year (or 1 day) before impact, could (or would) any stand-on mission be deployed to nullify the threat? A single DE-STAR system of modest size and flexibility would have been capable of eliminating the threats from both 2012 DA14 (in about a day

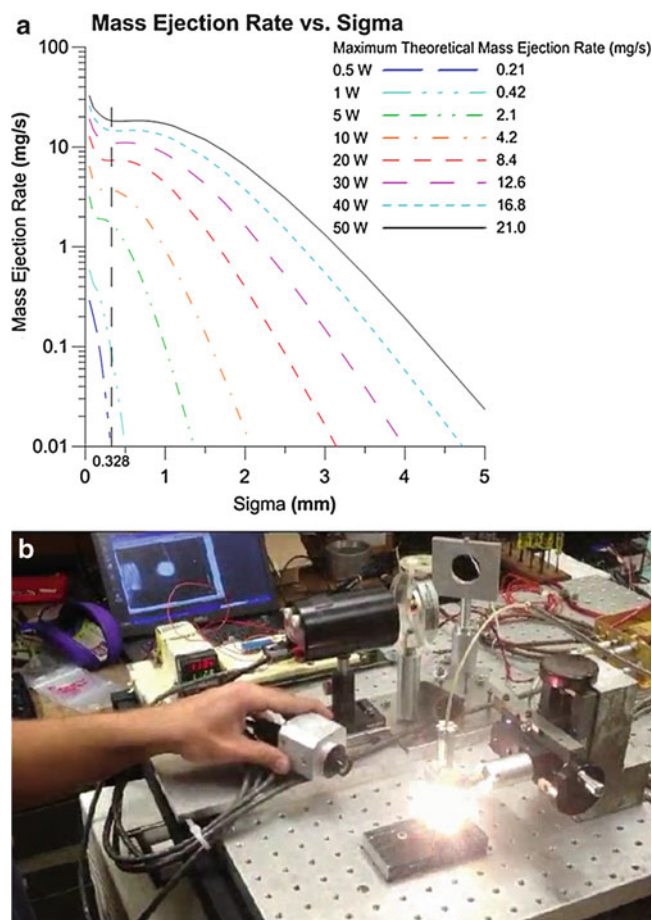


Fig. 24 (a) 2D simulation with laboratory test parameters. Similar to Fig. 14 but set for lab testing. Plot is of expected mass ejection versus sigma (Gaussian beam) for various power levels. Measured sigma based on hole size in targets is less than 330 μm . Sample is assumed to be SiO_2 . (b) Picture of test system. Small camera is an 8–12 μm FLIR IR microbolometer unit. Sample is sand

of targeting) and the Chelyabinsk impactor in less than 1 h of targeting (assuming prior detection by surveillance efforts). In particular, a functioning DE-STAR would be capable of mounting very rapid responses to newly discovered objects that have no chance of being mitigated by stand-on systems. As previously stated, a single orbiting DE-STAR of sufficient size could be designed to simultaneously engage multiple approaching objects. Unlike stand-on approaches, DE-STAR could be tested and validated at every stage of development, considerably increasing confidence that the system would succeed when needed the most. Since DE-STAR would be capable of addressing other scientific goals, development costs could also be spread across multiple scientific budgets.

The standoff strategy of DE-STAR has many obvious and critical advantages over stand-on schemes currently being considered for asteroid impact avoidance. It is worth the effort to explore the many issues associated with designing, developing, and deploying an orbiting DE-STAR. In this chapter, baseline system requirements and architecture are considered; cost-benefit analysis will be addressed in future work.

Other Uses for DE-STAR

Summary of Other Uses

DE-STAR is a standoff directed energy system and there a number of other uses that are possible. Some of these alternative uses are explored in detail. Clearly if it is possible to “laser machine” on solar system scales, this brings up some thought-provoking discussions.

Some of the more mundane ideas are:

- Space debris mitigation – a small unit (DE-STAR 1) is extremely effective against space debris. A unit attached to the ISS would be very useful in clearing out orbital debris.
- A LIDAR mode for refining the orbital parameters of asteroid. DE-STAR is extremely bright and makes an excellent “flashlight” to target asteroids in order to detect and refine their positions (Riley et al. 2014). As an aid to existing efforts, active illumination can be quite useful. The narrow bandwidth allows for extremely low-background searches as well as Doppler velocity determination.
- Standoff composition analysis – the bright heated spot might be used as a backlight to determine asteroid ejecta composition. An analysis is underway to see what is feasible.
- Orbital capture – modifying the orbits of asteroids may allow for easier capture if desired.
- Beam power to distant probes – the system can be used to beam power to very distant spacecraft. At 1 AU, the flux is 70 MW/m^2 or about 50,000 times the flux of the Sun. At the edge of the solar system (30 AU), it is about 80 kW/m^2 . At 225 AU, the beam is about as bright as the Sun is above the Earth’s atmosphere. Similarly it could be used to provide power to distant outposts on Mars or the Moon or literally to machine on the lunar surface (or possibly Mars). The latter would be a complex sociological and geopolitical discussion no doubt.
- Spacecraft rail gun mode – while photon pressure is modest, it is constant until the beam diverges to be larger than the reflector. In a companion paper, Bible et al. (2013) discuss using this mode to propel spacecraft at mildly relativistic speeds. For example, a 100, 1,000, and 10,000 kg spacecraft with a 30 m diameter (9 kg – 10 μm thick multilayer dielectric) reflector will reach 1 AU (~Mars) in 3,10,30 days. Stopping is an issue! The 100 kg craft will be going at 0.4 % c at a 1 AU and 0.6 % c at the edge of the solar system. This is 1,800 km/s at the edge of the solar system with just a 30 m reflector. This speed is far greater than the galactic escape speed and nearly 100 times faster than the Voyager spacecraft. If a reflector could be built to intercept the beam out to the edge of the solar system (900 m diameter), the same craft would be going 2 % at the edge of the solar system and 3 % if illumination stayed on for about 2 months. It is not currently known how to build km-class reflectors that have low enough mass, though it appears feasible to make 30 m and 100 m reflectors. There is work on graphene sheets that may allow for future extremely large- and extremely low-mass reflectors that may allow for fully relativistic speeds. Future generation may build even larger DE-STAR 5 and 6 units to allow highly relativistic probes.
- Laser-driven launch and boosters – a high-power ground-based DE-STAR could be used for launch purposes when used as an ablation (Campbell et al. 2003) or plume thrust driver. Similarly for orbital boost from low Earth orbit (LEO) to geosynchronous Earth orbit (GEO) and beyond, a DE-STAR could be extremely useful.
- SPS mode – beam power to the ground via microwave or mm wave. The system would produce about 100 GW (electrical). The US consumption is about 440 GW (electrical) average (1,400 W/person – average).

- Interstellar beacon – DE-STAR appears brighter than the brightest nighttime star at 1,000 ly (typical distance to Kepler-discovered exoplanets). Optical search for extraterrestrial intelligence (SETI) use is being explored for both transmit and receive modes.
- Ultrahigh-speed IR communications – the calculated data rates for DE-STAR to long-range, even interstellar probes are enormous with Mb/s speeds back to Earth from probes at the nearest stars for relatively small spacecraft transmitters and reflectors.

Conclusion

Directed energy systems represent a solution to planetary defense against asteroids and comets that threaten Earth. The same system can be used for a multitude of other purposes and thus is not a single-use system waiting for an asteroid. Its use in active illumination, remote composition analysis, spacecraft propulsion, space debris mitigation, and SPS (Space Power Satellite) could more than justify its cost let alone its ability to protect the Earth from catastrophe. Being modular and scalable, the DE-STAR can be built in stages as technology progresses. Small DE-STAR 0 (1 m) and DE-STAR 1 (10 m) class units can be built, tested, and even flown on suborbital platforms to test the basic concepts as small orbital versions are built. The technology is improving rapidly and already nearly “there” in terms of conversion efficiency. There are many other uses that are not discussed here for brevity. A logical progression is possible from the smaller DE-STAR ground and suborbital units to small orbital units as the technology improves and laser mass power density improves until it is possible to deploy a full-scale system such as a DE-STAR 4. As humanity becomes more technologically advanced, even larger systems can be envisioned including systems that will allow the first interstellar probes.

Acknowledgments

The funding from the NASA California Space Grant NASA NNX10AT93H in support of this research is gratefully acknowledged. The assistance from the Zemax support team for the Zemax optical simulations is also appreciated.

Cross-References

- ▶ [Asteroid Redirect Mission by NASA](#)
- ▶ [Comet Shoemaker-Levy 9](#)
- ▶ [Deep Impact and Related Missions](#)
- ▶ [Deflecting or Disrupting a Threatening Object](#)
- ▶ [Economic Challenges of Financing Planetary Defense](#)
- ▶ [ESA’s PHA’s Program](#)
- ▶ [Global Leadership and Strategies for Planetary Defense](#)
- ▶ [Hazard of Orbital Debris](#)
- ▶ [International Cooperation and Collaboration in Planetary Defense Efforts](#)
- ▶ [Keyholes](#)
- ▶ [Minor Planet Center](#)
- ▶ [Nature of the Threats and Historical Patterns of Occurrence](#)

- ▶ NEO Shield Program of the EU
- ▶ OSIRIS-REx Asteroid Sample Return Mission
- ▶ Planetary Defense, Global Cooperation and World Peace
- ▶ Possible Institutional and Financial Arrangements for Active Removal of Orbital Space Debris
- ▶ Potentially Hazardous Asteroids and Comets
- ▶ Private Initiatives: The Sentinel Project
- ▶ Spaceguard Survey by NASA: Behind Schedule and Seeking to Increase Mapping Capabilities
- ▶ Strategic Issues Involved with Planetary Defensive Systems and Active Debris Removal Systems
- ▶ The B612 Foundation's Sentinel Space Telescope to Create a 100 Year Warning Program
- ▶ The NASA Sentry Risk Table
- ▶ The Yarkovsky Effect
- ▶ US Based Systems (MPC, Smithsonian, MIT Linear System, NEAT, Spacewatch, LONEOS, Catalina)
- ▶ Wide-Field Infrared Survey Explorer (WISE) and NEOWise

References

- Belton MJS, Morgan TH, Samarasinha NH, Yeomans DK (eds) (2004) Mitigation of hazardous comets and asteroids. Cambridge University Press, New York
- Bible J, Johansson I, Hughes GB, Lubin PM (2013) Relativistic propulsion using directed energy. In: Taylor EW, Cardimona DA (eds) Nanophotonics and macrophotonics for space environments VII. Proceedings of SPIE, vol 8876, 887605
- Binzel RP, Rivkin AS, Thomas CA, Vernazza P, Burbine TH, DeMeo FE, Bus SJ, Tokunaga AT, Birlan M (2009) Spectral properties and composition of potentially hazardous asteroid (99942) Apophis. *Icarus* 200:480–485
- Campbell JW, Phipps C, Smalley L, Reilly J, Boccio D (2003) The impact imperative: laser ablation for deflecting asteroids, meteoroids, and comets from impacting the earth. In: BEAMED ENERGY PROPULSION: first international symposium on beamed energy propulsion 664(1), AIP Publishing, Melville, pp 509–522
- Colombo C, Vasile M, Radice G (2009) Semi-analytical solution for the optimal low-thrust deflection of near-earth objects. *J Guid Control Dyn* 32(3):796–809
- Conway BA (2004) Optimal interception and deflection of Earth-approaching asteroids using low-thrust electric propulsion. In: Belton MJS, Morgan TH, Samarasinha N, Yeomans DK (eds) Mitigation of hazardous comets and asteroids. Cambridge University Press, New York, pp 292–312
- Cuartielles JPS et al (2007) A multi-criteria assessment of deflection methods for dangerous NEOs. In: New trends in astrodynamics and applications III. AIP conference proceedings 886(1), American Institute of Physics/Springer, New York, pp 317–336
- D'Addario LR (2008) Combining loss of a transmitting array due to phase errors. IPN Progress Report 42-175, Nov 2008
- Delbò M, Cellino A, Tedesco EF (2007) Albedo and size determination of potentially hazardous asteroids: (99942) Apophis. *Icarus* 188:266–270
- Fan TY (2005) Laser beam combining for high-power, high-radiance sources. *IEEE J Sel Top Quantum Electron* 11:567
- Gibbings MA, Hopkins JM, Burns D, Vasile M (2011) On testing laser ablation processes for asteroid deflection, 2011 IAA planetary defense conference, Bucharest

- Gritzner C, Kahle R (2004) Mitigation technologies and their requirements. In: Belton MJS et al (eds) *Mitigation of hazardous comets and asteroids*, vol 1. Cambridge University Press, New York, p 167
- Harris AW (1998) A thermal model for near-Earth asteroids. *Icarus* 131:291–301
- Hughes GB, Lubin P, Bible J, Bublitz J, Arriola J, Motta C, Suen J, Johansson I, Riley J, Sarvian N, Wu J, Milich A, Oleson M, Pryor M (2013) DE-STAR: phased-array laser technology for planetary defense and other scientific purposes (Keynote Paper). In: Taylor EW, Cardimona DA (eds) *Nanophotonics and macrophotonics for space environments VII*. Proceedings of SPIE, vol 8876, 88760J
- Hughes GB, Lubin P, Griswold J, Bozinni D, O’Neill H, Meinhold P, Suen J, Bible J, Riley J, Johansson I, Pryor M, Kangas M (2014) Optical modeling for a laser phased-array directed energy system (Invited Paper). In: Taylor EW, Cardimona DA (eds) *Nanophotonics and macrophotonics for space environments VIII*. Proceedings of SPIE, vol 9226
- Hyland DC, Altwajjry HA, Ge S, Margulieux R, Doyle J, Sandberg J, Young B, Bai X, Lopez J, Satak N (2010) A permanently-acting NEA damage mitigation technique via the Yarkovsky effect. *Cosm Res* 48(5):430–436
- Johansson I, Tsareva T, Griswold J, Lubin P, Hughes GB, O’Neill H, Meinhold P, Suen J, Zhang Q, Riley J, Walsh K, Mellis C, Brashears T, Bollag J, Matthew S, Bible J (2014) Effects of asteroid rotation on directed energy deflection. In: Taylor EW, Cardimona DA (eds) *Nanophotonics and macrophotonics for space environments VIII*. Proceedings of SPIE, vol 9226
- Kahle R, Hahn G, Kührt E (2006) Optimal deflection of NEOs en route of collision with the Earth. *Icarus* 182(2):482–488
- Koenig JD, Chyba CF (2007) Impact deflection of potentially hazardous asteroids using current launch vehicles. *Sci Glob Secur* 15(1):57–83
- Kosmo K, Pryor M, Lubin P, Hughes GB, O’Neill H, Meinhold P, Suen JC, Riley J, Griswold J, Cook BV, Johansson IE, Zhang Q, Walsh K, Melis C, Kangas M, Bible J, Motta, Brashears, T., Mathew S, Bollag J (2014) DE-STARLITE – a practical planetary defense mission. In: Taylor EW, Cardimona DA (eds) *Nanophotonics and macrophotonics for space environments VIII*. Proceedings of SPIE, vol 9226
- Lu ET, Love SG (2005) A gravitational tractor for towing asteroids. arXiv preprint astro-ph/0509595
- Lubin P, Hughes GB, Bible J, Bublitz J, Arriola J, Motta C, Suen J, Johansson I, Riley J, Sarvian N, Clayton-Warwick D, Wu J, Milich A, Oleson M, Pryor M, Krogan P, Kangas M (2013) Directed energy planetary defense (Plenary Paper). In: Taylor EW, Cardimona DA (eds) *Nanophotonics and macrophotonics for space environments VII*. Proceedings of SPIE, vol 8876, 887602
- Lubin P, Hughes GB, Bible J, Bublitz J, Arriola J, Motta C, Suen J, Johansson I, Riley J, Sarvian N, Clayton-Warwick D, Wu J, Milich A, Oleson M, Pryor M, Krogen P, Kangas M, O’Neill H (2014) Toward directed energy planetary defense. *Opt Eng* 53(2):025103-1–025103-18. doi:10.1117/1.OE.53.2.025103
- Maddock C, Cuartielles JPS, Vasile M, Radice G (2007) Comparison of single and multi-spacecraft configurations for NEA deflection by solar sublimation. In: AIP conference proceedings, vol 886. AIP Publishing, Melville, p 303
- McInnes CR (2004) Deflection of near-Earth asteroids by kinetic energy impacts from retrograde orbits. *Planet Space Sci* 52(7):587–590
- Melosh HJ, Ryan EV (1997) Asteroids: shattered but not dispersed. *Icarus* 129(2):562–564
- Morrison D, Harris AW, Sommer G, Chapman CR, Carusi A (2002) Dealing with the impact hazard. In: Bottke W et al (eds) *Asteroids III*. University of Arizona Press, Tucson, pp 739–754

- Mueller M (2007) Surface properties of asteroids from mid-infrared observations and thermophysical modeling. arXiv preprint arXiv:1208.3993
- Mueller M, Harris AW, Fitzsimmons A (1989) Size, albedo, and taxonomic type of potential spacecraft target Asteroid (10302) 1989 ML. *Icarus* 187:611–615
- Olds J, Charania A, Schaffer MG (2007) Multiple mass drivers as an option for asteroid deflection missions. In: 2007 Planetary defense conference, Washington, DC, Paper, pp S3–S7
- Riley J, Lubin P, Hughes GB, O’Neill H, Meinhold P, Suen J, Bible J, Johansson I, Griswold J, Cook B (2015) Directed energy active illumination for near-Earth object detection. *J Astron Telescopes Instrum Syst* (accepted)
- Schweickart R, Chapman C, Durda D, Hut P (2006) Threat mitigation: the gravity tractor. arXiv preprint physics/0608157
- Vasile M, Maddock CA (2010) On the deflection of asteroids with mirrors. *Celestial Mech Dyn Astron* 107(1):265–284
- Vorontsov MA, Weyrauch T, Beresnev LA, Carhart GW, Liu L, Aschenback K (2009) Adaptive array of phase-locked fiber collimators: analysis and experimental demonstration. *IEEE J Sel Top Quantum Electron* 15:269
- Walker R, Izzo D, de Negueruela C, Summerer L, Ayre M, Vasile M (2005) Concepts for near-Earth asteroid deflection using spacecraft with advanced nuclear and solar electric propulsion systems. *J Br Interplanet Soc* 58(7–8):268–278
- Warner BD, Harris AW, Pravec P (2009) The asteroid lightcurve database. *Icarus* 202:134–146
- Wie B (2007) Hovering control of a solar sail gravity tractor spacecraft for asteroid deflection. In: Proceedings of the 17th AAS/AIAA space flight mechanics meeting, AAS, Washington, DC, vol 7, p 145